
Hamiltonian Monte Carlo with Asymmetrical Momentum Distributions

Soumyadip Ghosh
IBM Research

Yingdong Lu
IBM Research

Tomasz Nowicki
IBM Research

Abstract

Existing rigorous convergence guarantees for the Hamiltonian Monte Carlo (HMC) algorithm use Gaussian auxiliary momentum variables, which are crucially symmetrically distributed. We present a novel convergence analysis for HMC utilizing new analytic and probabilistic arguments. The convergence is rigorously established under significantly weaker conditions, which among others allow for general auxiliary distributions. In our framework, we show that plain HMC with asymmetrical momentum distributions breaks a key self-adjointness requirement. We propose a modified version that we call the Alternating Direction HMC (AD-HMC). Sufficient conditions are established under which AD-HMC exhibits geometric convergence in Wasserstein distance. Numerical experiments suggest that AD-HMC can show improved performance over HMC with Gaussian auxiliaries.

1 Introduction

Hamiltonian Monte Carlo (HMC) belongs to the wider class of Markov Chain Monte Carlo (MCMC) algorithms (Hastings, 1970; Gelfand and Smith, 1990) that approximate the difficult-to-compute density of a target probability measure by running a Markov chain whose invariant measure coincides with the target distribution. Let $f(q)$ denote the target density of interest. Define its support to be on a metric space $(\mathbb{Q}, \mathfrak{d})$, where we will assume \mathbb{Q} is, typically, a Euclidean space \mathbb{R}^m for some positive integer m and \mathfrak{d} is a metric in \mathbb{Q} .

The $f(q)$ is of form $f(q) = \hat{f}(q)/C$, where $\hat{f}(q)$ is easily

queried, but to completely characterize $f(q)$ we need to know the normalizing constant $C = \int_{\mathbb{Q}} \hat{f}(q) dq$, for example to compute expectations. This is a core problem in modern statistics, and forms a fundamental operation in many applications in machine/deep learning. For instance, in frequentist statistics, it relates to estimating coverage of a statistic using likelihood over data space. In Bayesian statistics, it can be generically stated as inferring the posterior distribution $f(q|x)$ of (unobservable) latent variables q given observations x from a user-modeled joint density $f(q, x)$. The inference target is $f(q|x) = f(q, x)/f(x)$, where the exact marginal $f(x) = \int f(q, x) dq$ is usually hard to compute directly.

This motivates the wide use of MCMC in applications such as statistical inference (Robert and Casella, 2004), inverse problems (Stuart, 2010), artificial intelligence (Andrieu et al., 2003) and molecular dynamics (Lelievre et al., 2010). The early success of the MCMC approach can be attributed to simple, elegant and provably convergent algorithms such as the Metropolis-Hastings method (Hastings, 1970), in which a user chosen auxiliary distribution and an acceptance/rejection mechanism helps pick and accept candidate samples as being from $f(q)$. But MCMC algorithms suffer from slow convergence in high dimensional statistical computing in fields like molecular dynamics and artificial intelligence.

Sample generation in the standard HMC (Algorithm 1) is driven by a dynamical system. Write the energy of the target distribution as $U(q) = -\log f(q)$. The user chooses an auxiliary set of *momentum* variables in space \mathbb{P} , which is also \mathbb{R}^m . The momentum p is sampled from a probability measure with density function $\mathfrak{g}(p) = e^{-V(p)}$, referred to as the *momentum* or *auxiliary* distribution with $V(p)$ its *kinetic* energy. In each iteration, the HMC Algorithm 1 spreads (or lifts) the current iterate $q \rightarrow (q, p)$, where p is sampled independently from $\mathfrak{g}(p)$. Hamiltonian dynamics with energy $H(q, p) = U(q) + V(p)$ are used to define the (deterministic) transformation $\mathcal{R} : (q, p) \mapsto (Q(T), P(T))$ with a pre-selected time T . It preserves $H(q, p)$, the total energy or Hamiltonian of the system. The P variables are then dropped by projecting $(Q(T), P(T)) \mapsto Q(T)$

to obtain next iterate. The terminology of q and p being the position and momentum variables, and $H(q, p)$ corresponding to the energy arose in physics applications, where HMC first saw wide-spread use (Duane et al., 1987).

Algorithm 1 Standard HMC

Initialization: potential energy $U(q)$, kinetic energy $V(p)$, initial iterate set $h_0 = (q_{01}, \dots, q_{0K})$, trajectory length T , total number of iterations N

for $n = 1, \dots, N$ **do**

for $k = 1, \dots, K$ **do**

 Set $q_0 \leftarrow q_{(n-1)k}$

 Sample: $p_0 \sim \mathbf{g}(p)$

 Lift: $(q_0, p_0) \leftarrow q_0$

 Apply Hamiltonian motion for length $+T$: $(Q(T), P(T)) \leftarrow (q_0, p_0)$

 Project: $q_1 \leftarrow Q(T)$

 Set $q_{nk} \leftarrow q_1$

end for

 Set $h_n = (q_{n1}, \dots, q_{nK})$

end for

Return $h_N = (q_{N1}, \dots, q_{NK})$

The power of HMC stems from the energy-preserving property when obtaining the candidate solutions even for large Hamiltonian moves, since this also preserves the joint density of (q, p) and hence (if the motion is exactly implemented) no new samples are rejected. This leads to its relatively higher effectiveness compared to classical MCMC even in the high dimensional settings used in deep learning with neural networks (Neal, 1993; Gelman et al., 2013; Jasche and Kitaura, 2010; Betancourt et al., 2017). With the rise of high-performance software implementations such as Stan (Carpenter et al., 2017; Team, 2017), the method has now become a pervasive tool across many scientific, medical, and industrial applications.

Role of Momentum Distribution. The kinetic energy $V(p)$ is typically symmetric and quadratic: $V(p) \propto p^t M^{-1} p$, and so the momentum p is distributed as a Gaussian distribution. A good choice for M is the Hessian of $U(q)$. Betancourt et al. (2017) note that if $U(q)$ is Gaussian, then the choice of M as the inverse of the covariance of q under $f(q)$, leads to the optimal de-skewing and regularization of contours of the Hamiltonian motion. Consequently, this prevents the uncontrolled build up of error in practical discretized approximations of Hamiltonian dynamics implemented on a computer. When the $U(q)$ is non-Gaussian, existing convergence proofs of HMC do not allow the momentum distribution to be asymmetric. As a workaround, the Riemannian-Gaussian (Girolami and Calderhead, 2011) kinetic energy $V(p|q) \propto p^t M(q)^{-1} p$ is used, where the $M(q) = \nabla^2 U(q)$ the Hessian of $U(q)$. So, the kinetic energy is updated dynamically by continually estimating

at each q the “local” Hessian directly (or approximating covariance of recent samples) to locally regularize the Hamiltonian motion curvature.

Limitations of Prior Results. A rich literature has emerged on the important theoretical problem of when and how fast the HMC algorithm with (conditional) Gaussian $V(p)$ converges. Of particular interest has been the conditions under which geometric convergence can be ensured, which has been achieved through different approaches such as comparison theorems for differential equations (Chen and Vempala, 2019), Harris recurrence techniques (Bou-Rabee and Sanz-Serna, 2017) and coupling (Bou-Rabee et al., 2020). Some of the various conditions identified for geometric ergodicity of HMC are not easy to verify (e.g. (Bou-Rabee and Sanz-Serna, 2017)), some (Durmus et al., 2017; Mangoubi and Smith, 2019; Livingstone et al., 2019) cannot lead to explicit expression of the convergence rate on the HMC parameters, while others (Bou-Rabee et al., 2020) heavily depends on delicate tricks for Gaussian $V(p)$ distributions, and require log-concave properties of the target density function.

The existing approaches crucially use the fact that under appropriate conditions on the Hamiltonian function, the Markov chains starting from any two fixed points in the state space would eventually result in iterated distributions that are (under some well-defined distributional metric) closer than the two origination points. Recent advances in the understanding of general Markov operators from the perspective of optimal transportation shed clearer light on this phenomenon, see e.g. Ollivier (2009) and Joulin and Ollivier (2010). In this approach, the geometric convergence in Wasserstein metric of the Markov chain is quantified by the coarse Ricci curvature, a geometric concept that provides a second order characterization of movements in the probability measure space. Importantly, the curvature approach lets us produce quantitative characterization of the Markov chain through detailed calculations of the trajectories in the Hamiltonian system.

Contributions. The main thrust of our paper is in the presentation of a new set of analysis techniques for HMC style algorithms. In contrast to most previous work that treats the convergence of iterates $\{q_n\}$ of Algorithm 1, we analyse the convergence of the corresponding induced densities $\{h_n\}$ on a properly defined function space. This functional convergence approach allows us, in Sec. 2, to identify key properties of Hamiltonian motions that are sufficient for convergence. Seen in this light, the standard HMC operator (defined in Sec. 3) with an asymmetric momentum distribution is not self-adjoint, a characteristic that is essential to the proof of convergence. The modified Alternating Direction HMC (AD-HMC) Algorithm 2 rectifies this

by applying the HMC operator and its adjoint in alternating steps, amounting to taking Hamiltonian motion in forward and backward directions. Theorem 1 shows that AD-HMC converges strongly to $f(q)$ in the functional space. This significantly expands the class of HMC algorithms for which convergence is rigorously established, among others by dropping the symmetry restriction on momentum distributions. The proofs provide a simple and intuitive understanding of the working of HMC and illustrate *why* its iterates converge. Moreover, our observations on the functional and probabilistic structures of the algorithms lead to a significantly shortened presentation compared to previous work in the literature.

In Section 4.1, we establish that geometric convergence holds. In Theorem 2 the AD-HMC method with asymmetric $V(p)$ enjoys this rate under standard log-concavity conditions that are imposed on target $f(q)$ and auxiliary $g(p)$. The analysis technique here switches to using probabilistic arguments over measure spaces endowed with the Wasserstein metric. This shift allows us in Theorem 3 of Section 4.2 to generalize our analysis by relaxing the global conditions to only requiring that log-concavity hold outside a “small” set (defined in (3)). While we do not necessarily provide the tightest convergence rate estimate in comparison to existing results, our results focus on convergence in Wasserstein metric, which is not only a weaker notion hence covering more applications in practice but can also provide more robust bound for high dimensional problems as discovered in recent literature; see e.g. Hairer et al. (2011) and Durmus and Moulines (2015). The Hamiltonian dynamics in Algorithm 2 are implemented by discrete numerical approximations such as the leapfrog integrator (Leimkuhler and Reich, 2004); Section 4.3 proves in Theorem 4 that such practical discretization schemes also converge geometrically if the error it produces can be uniformly bounded.

Section 5 describes our initial numerical experiments that suggest the potential benefit of considering asymmetrical momentum distributions. As discussed earlier, a popular technique to speed up standard HMC methods is to dynamically update the covariance matrix of the auxiliary distribution with either the directly computed Hessian $\nabla^2 U(q)$ or its approximation from the covariance of samples (see ‘**adapt-single**’ heuristic in Sec. 5). We propose an alternate adaptive scheme, ‘**adapt-many**’, that utilises the AD-HMC algorithm to dynamically construct $g(p)$ as a general mixture of Gaussians with components that provide adequate coverage of the target. In a three-dimensional simulated dataset example where the target $f(q)$ is chosen to be full dimensional and significantly asymmetric with wide variance in $\nabla^2 U(q)$, we demonstrate that

the AD-HMC based heuristic significantly outperforms standard HMC with adaptively learnt Gaussian distributions. On a public domain Bayesian logistic regression dataset, the AD-HMC ‘**adapt-many**’ and HMC ‘**adapt-single**’ performs similarly.

The ‘**adapt-many**’ heuristic and its examples provided in Section 5 motivate the use of general auxiliary distributions and display the great potential of AD-HMC. An exhaustive study of the practical, versatile uses of AD-HMC is beyond the scope of this paper. We can be certain that additional applications for asymmetric auxiliaries will become apparent as the literature delves into AD-HMC further, and we intend to further pursue deeper exhaustive investigations along these lines.

2 Preliminaries

As noted, the HMC iterates are formally defined over a state space \mathbb{Q} , and we assume that the initial state is sampled from an arbitrary distribution that is absolutely continuous with respect to a reference measure on \mathbb{Q} , which in most of the cases will be the Lebesgue measure on a Euclidean space.

Each step of HMC applies a Hamiltonian motion to a joint sample $(q, p) \mapsto (Q(T), P(T))$, which is the evaluation of the solution to the following system of differential equations at a fixed time $T > 0$,

$$\dot{Q}(t) = \frac{\partial H}{\partial p}, \dot{P}(t) = -\frac{\partial H}{\partial q}, (Q(0), P(0)) = (q, p). \quad (1)$$

The solution represents the position and momentum in the Hamiltonian conservation system for time $t \in [0, T]$. Since the parameter T will remain fixed in this paper, we will omit it when there is no confusion. Furthermore, denote $\mathcal{R}(q, p)$ as the map $(q, p) \mapsto (Q, P)$. The measurable motion \mathcal{R} is assumed to be invertible, which corresponds to being able to go back in time and have two *invariance properties*: (1) $f(Q) \cdot g(P) = f(q) \cdot g(p)$ (conservation of the Hamiltonian energy) and (2) for any integrable function $A : \mathbb{Q} \times \mathbb{P} \rightarrow \mathbb{R}$ we have $\iint_{\mathbb{Q} \times \mathbb{P}} A \circ \mathcal{R} d(q, p) = \iint_{\mathbb{Q} \times \mathbb{P}} A d(q, p)$ (conservation of Lebesgue measure by the Hamiltonian motion). Additionally we assume that the motion is irreducible (ergodic), which means there are no nontrivial measurable invariant sets. For simplicity we assume a stronger *coverage property*: (3) $\mathcal{R}(q, \mathbb{P}) = \mathbb{Q}$ for (almost) every $q \in \mathbb{Q}$. This compactly represents (using a slight abuse of notation $\mathcal{R}(\cdot, \cdot)$) the property that every point in \mathbb{Q} can be reached from (almost) any $q \in \mathbb{Q}$ with a lift by an appropriate p for the motion \mathcal{R} in one step.

The evolution of iterates q is naturally modelled as a Markov chain. Next step depends only on the previous one and an independent and randomly generated momentum vector p . Hence, we can equivalently study the

evolution of the density functions of the Markov chain. Our HMC analysis combines a dynamical system on a functional space with methods in probability theory.

HMC as a Markov chain

Modeling the evolution of Algorithm 1 as a Markov chain defined on the space \mathbb{Q} , its transition probability can be defined as follows. Given the fixed parameter T and initial position $q \in \mathbb{Q}$, the map $\Pi_q := \mathfrak{m}_{\mathbb{Q}} \circ \mathcal{R}(q, \cdot) : \mathbb{P} \rightarrow \mathbb{Q}$, with $\mathfrak{m}_{\mathbb{Q}}$ being the usual projection from $\mathbb{Q} \times \mathbb{P}$ to \mathbb{Q} , is an onto map. Hence, for any given probability measure \mathfrak{G} on \mathbb{P} (with density $\mathfrak{g}(p) = e^{-V(p)}$), Π_q induces a push forward $(\Pi_q)_\#(\mathfrak{G})$, a probability measure on \mathbb{Q} defined as $(\Pi_q)_\#(\mathfrak{G})(A) = \mathfrak{G}(\Pi_q^{-1}(A))$ for any measurable set A , with $\Pi_q^{-1}(A)$ denoting its pre-image under Π_q . This push forward provides the transition probability for our Markov chain, $P(q, A) := (\Pi_q)_\#(\mathfrak{G})(A)$.

HMC as a Dynamical System

From an analytical point of view, the density function of a probability measure, well-defined when the measure is absolutely continuous with respect to the reference (Lebesgue) measure, can also be viewed as a member in a proper functional space. First, let the target measure on the space \mathbb{Q} (which we can assume to be its support) be expressed as a density \mathfrak{f} with respect to the reference measure dq on \mathbb{Q} . The abstract (or ideal) HMC uses an auxiliary measure with a density \mathfrak{g} on the space \mathbb{P} with respect to the reference measure dp there. A step of HMC is a realization of an operator \mathcal{T} acting on the densities $h : \mathbb{Q} \rightarrow \mathbb{R}$ belonging to $L^2_{\mathfrak{f}} := \{h : \|h\|_{\mathfrak{f}}^2 = \int h^2/\mathfrak{f} < \infty\}$, where the integration is with respect to the reference measure dq . To simplify notation we shall skip the subscript \mathfrak{f} and write L^2 and $\|h\|^2$. The operator \mathcal{T} first constructs the joint distribution $h(q)\mathfrak{g}(p)$ on $\mathbb{Q} \times \mathbb{P}$ (in the lifting step), then performs the Hamiltonian motion in the product space $(q, p) \mapsto (Q, P) = \mathcal{R}(q, p)$ producing a joint distribution $h(Q) \cdot \mathfrak{g}(P) = (h \cdot \mathfrak{g}) \circ \mathcal{R}(q, p)$ and finally projects this transported density along the direction of \mathbb{P} on its marginal on space \mathbb{Q} . More specifically,

$$\mathcal{T}h(q) = \int_{\mathbb{P}} (h \cdot \mathfrak{g}) \circ \mathcal{R}(q, p) dp = \int_{\mathbb{P}} h(Q)\mathfrak{g}(P) dp. \quad (2)$$

The progression of HMC algorithm applied to an initial density h can be expressed as the sequence of iterations of the operator $\mathcal{T}^n h$, where $\mathcal{T}^{n+1} = \mathcal{T} \circ \mathcal{T}^n$.

2.1 Notions of Convergence

With the Markov chain and dynamical system defined above, various notions of convergence need to be discussed for understanding the main results of the pa-

per. For a Markov chain, it is well known that, under proper assumptions, there exists a probability measure μ^∞ that is invariant under the push forward $(\Pi_q)_\#$, hence named invariant measure. Furthermore, in typical probabilistic literature, $\lim_{n \rightarrow \infty} d_{TV}(\mu_n, \mu^\infty) = 0$, where $\mu_n = ((\Pi_q)_\#)^n \mu_0$ for some initial probability μ_0 , and d_{TV} denotes the *total variational distance* between two measures, $d_{TV}(\mu, \nu) = \sup_A |\mu(A) - \nu(A)|$ with the supremum taken over all the sets in the σ -field where the probability measures are defined. In terms of the HMC notation, the measures μ_n and μ^∞ can be viewed to have densities h_n and \mathfrak{f} .

The total variational distance has been extensively studied in statistics and probability, and has close connections to other distance metrics of probability measures such as the Kullback-Leibler divergence. See Definition 1 of the family of metrics (Joulin and Ollivier, 2010) of closeness of probability measures. It is however beneficial and sometimes more convenient to consider convergence under the Wasserstein distance.

Definition 1. For any two measures μ and ν on metric space $(\mathbb{Q}, \mathfrak{d})$, the Wasserstein distance $W_p(\mu, \nu)$ for $p > 0$ is defined as,

$$W_p(\mu, \nu) = \inf_{\gamma \in \Gamma(\mu, \nu)} \left[\int_{\mathbb{Q} \times \mathbb{Q}} \mathfrak{d}^p(x, y) \gamma(dx, dy) \right]^{\frac{1}{p}}, \quad (3)$$

where $\Gamma(\mu, \nu)$ denotes the set of measures on $\mathbb{Q} \times \mathbb{Q}$ that project on μ and ν .

A closely related concept is that of the coarse Ricci curvature of a Markov operator, developed in Ollivier (2009) and Joulin and Ollivier (2010). Ricci curvature of a Riemannian manifold is interpreted as a measure of deformation along parallel transformations.

Definition 2. On the space \mathbb{Q} , with the Markov operator \mathcal{P} , for each pair $(q_1, q_2) \in \mathbb{Q} \times \mathbb{Q}$, the coarse Ricci curvature $\kappa(q_1, q_2)$ in the direction of (q_1, q_2) , is defined as,

$$\kappa(q_1, q_2) := 1 - \frac{W_1(\mu(q_1), \mu(q_2))}{\mathfrak{d}(q_1, q_2)},$$

where $\mu(q)$ denotes the probability distribution of the Markov chain governed by \mathcal{P} with initial state q .

Denote $\kappa := \inf_{(q_1, q_2) \in \mathbb{Q} \times \mathbb{Q}} \kappa(q_1, q_2)$. It is demonstrated in Ollivier (2009) that $\kappa > 0$ implies that the corresponding Markov recursion converges geometrically.

From the analytical viewpoint, the convergence of the HMC is studied in terms of convergence of density functions in a proper functional space. In particular, the L^2 space defined previously with respect to the reciprocal of the density function \mathfrak{f} has been found to be very useful in establishing the convergence for a variety

of iterative operators, see e.g. Markowich and Villani (2000). The space L^2 has a natural scalar product $\langle a, b \rangle = \int ab/\mathfrak{f}$. Hence, the (strong) convergence in L^2 for a sequence of functions h_n to a function h is defined by $\lim_{n \rightarrow \infty} \|h_n - h\| = 0$, and the weak convergence is defined as $\lim_{n \rightarrow \infty} \langle h_n - h, a \rangle = 0$, for any $a \in L^2$. In Chen (2000), it is shown that L^2 geometric convergence is equivalent to geometric ergodicity, which is a well studied property in the Markov chain literature.

3 The Alternating Direction HMC

In the space L^2 , the *adjoint* operator \mathcal{T}^\dagger to \mathcal{T} is characterized by $\langle \mathcal{T}a, b \rangle = \langle a, \mathcal{T}^\dagger b \rangle$ for any $a, b \in L^2$. Note that by the invariance properties described after the definition of the Hamiltonian (1), $\mathcal{T}^\dagger h = \int_{\mathbb{P}} (h \cdot \mathfrak{g}) \circ \mathcal{R}^{-1}$. A *self-adjoint* operator satisfies $\mathcal{T}^\dagger = \mathcal{T}$, and for Hamiltonian motion a sufficient condition for self-adjointness is that the auxiliary distribution is symmetric $\mathfrak{g}(p) = \mathfrak{g}(-p)$. Self-adjointness is crucial to the convergence result in Theorem 1 below.

In case the operator \mathcal{T} is not self-adjoint (for example when $\mathfrak{g}(p)$ is asymmetrical) we use a method with $\mathcal{T}_a = \mathcal{T}^\dagger \circ \mathcal{T}$ in place of \mathcal{T} . Algorithm 2 presents the proposed Alternating Direction Hamiltonian Monte Carlo (AD-HMC) method. It is a modification of the standard HMC Algorithm 1 where forward motion of size T is followed by backward motion (with fresh momentum samples) of size $-T$, where signs of the motion equations (1) are reversed. The AD-HMC operator \mathcal{T}_a has both invariance properties and is self-adjoint.

Algorithm 2 Alternating Direction HMC

Initialization: potential energy $U(q)$, kinetic energy $V(q)$, initial iterate set $h_0 = (q_{01}, \dots, q_{0K})$, trajectory length T , total number of iterations N
for $n = 1, \dots, N$ **do**
 for $k = 1, \dots, K$ **do**
 Set $q_0 \leftarrow q_{(n-1)k}$
 Sample: $p_0 \sim \mathfrak{g}(p)$ *{forward motion}*
 Lift: $(q_0, p_0) \leftarrow q_0$
 Apply Hamiltonian motion for length $+T$:
 $(Q(T), P(T)) \leftarrow (q_0, p_0)$
 Project: $q_{0'} \leftarrow Q(T)$
 Sample: $p_{0'} \sim \mathfrak{g}(p)$ *{backward motion}*
 Lift: $(q_{0'}, p_{0'}) \leftarrow q_{0'}$
 Apply Hamiltonian motion for length $-T$:
 $(Q(-T), P(-T)) \leftarrow (q_{0'}, p_{0'})$
 Project: $q_1 \leftarrow Q(-T)$
 Set $q_{nk} \leftarrow q_1$
 end for
 Set $h_n = (q_{n1}, \dots, q_{nK})$
end for
Return $h_N = (q_{N1}, \dots, q_{NK})$

Theorem 1. *Let the motion \mathcal{R} that defines the operator \mathcal{T} have invariance and coverage properties. Then for any $h \in L^2$ the sequence of alternating iterations $\mathcal{T}_a^n h$ converges strongly to the fix point $\alpha \mathfrak{f}$, where $\alpha = \int h/\int \mathfrak{f}$. If additionally \mathcal{T} is self-adjoint itself then $\mathcal{T}^n h$ converges strongly to $\alpha \mathfrak{f}$.*

For the proof of Theorem 1, detailed in Sec. A.1, we observe that \mathcal{T} is in fact an averaging map (Lemma 3), thus by the convexity of $x \mapsto x^2$ the norm decreases under \mathcal{T} : $\|\mathcal{T}h\| < \|h\|$ (Lemma 4), sharply unless (by coverage assumption) $h = \alpha \mathfrak{f}$. In the space L^2 , bounded sequences have weak accumulation points. Using self-adjointness we prove (Proposition 2) that each accumulation point of the sequence of iterations has the same norm and thus (Corollary 3) must be of form $\alpha \mathfrak{f}$, where the value α is deduced from integral invariance (Lemma 5). Hence the whole sequence converges. Meanwhile the proof of the convergence of the norms to the norm of the limit provides (Proposition 3) strong convergence.

4 Geometric Convergence in W_1

4.1 Global Condition on the Hessian

Recall that by the Ricci curvature arguments, the geometric convergence in the Wasserstein distance is established if the quantity $W_1(\mu(q_1), \mu(q_2))$ can be shown to be contracting comparing to the initial positions of the Hamiltonian motion. The precise calculation of $W_1(\mu(q_1), \mu(q_2))$ requires solving the well-known Monge-Ampère equation, a nonlinear elliptic equation whose solutions are hard to obtain, see e.g. Villani (2008). Here, we identify the conditions under which an upper bound can be derived to this important quantity, and this then leads to a lower bound to curvature κ , which is still a positive number, hence the geometric convergence of the Markov chain to its stationary distribution. While there exist several similar results for the geometric convergence of HMC, we believe that our proof provided here is among the simplest, and it provides important insights on the related dynamics that of independent interest.

Theorem 2. *If $\left| \frac{\partial Q}{\partial q} \right| \leq \beta$, for some $\beta \in (0, 1)$, where $|\cdot|$ denotes the operator norm for matrices, then the Markov recursion converges geometrically in the W_1 with a rate being at least $(1 - \beta)$.*

Proof of the theorem can be found in Sec. A.2. The bound $\left| \frac{\partial Q}{\partial q} \right| \leq \beta < 1$ is on the sensitivity of the Hamiltonian motion output Q on the starting point q , and applies for any momentum p . We will show below that this bound can be obtained if additional conditions are imposed on the form of the densities \mathfrak{f} and \mathfrak{g} .

As before, let $\mathbf{g}(p)$ have density $\exp(-V(p))$, and with Hamiltonian form $H(Q, P) = U(Q) + V(P)$, denote $V'' = \partial^2 H / \partial P^2$ and $U'' = \partial^2 H / \partial Q^2$. Define averages $\bar{V} = \bar{V}(t) = \frac{1}{t} \int_0^t V''(P(s)) ds$ and $\bar{U} = \bar{U}(t) = \frac{1}{t} \int_0^t U''(Q(s)) ds$, where P, Q are the solutions of (1). When \bar{V} and \bar{U} are symmetric and positive definite, denote $A = \sqrt{\bar{V}\bar{U}}$ and $B = \sqrt{\bar{U}\bar{V}}$. These roots exist because a unique symmetric positive square root exists for any symmetric positive operator, and a composition of two positive symmetric operators is also positive and has a well defined positive square root. Lemma 6 in the supplement Sec. A.3 studies the general evolution of the four initial-configuration dependence terms including the $\partial Q / \partial q(t)$. Proposition 1 below provides a solution of the evolution equations.

Proposition 1. *Assume that both the target and the auxiliary distributions are strictly log-concave over their domains. Then the solution of the evolution equation (6) (see Lemma 6 in Sec. A.3) is:*

$$\begin{pmatrix} \frac{\partial Q}{\partial q} & \frac{\partial Q}{\partial p} \\ \frac{\partial P}{\partial q} & \frac{\partial P}{\partial p} \end{pmatrix} (t) = \begin{pmatrix} \cos(tA) & t\bar{V} \operatorname{sinc}(tB) \\ -t\bar{U} \operatorname{sinc}(tA) & \cos(tB) \end{pmatrix}.$$

By logarithmic concavity and by continuity for each Q and P both V'' and U'' are positive symmetric operators, and so are their time averages \bar{V} and \bar{U} . The functions $\cos(x)$ and $\operatorname{sinc}(x) = x^{-1} \sin(x)$ used above are well defined by their power series, which are absolutely convergent for all bounded operators, the latter even when x^{-1} is not well defined.

Proof. The expression follows from standard calculations (see Lemma 7) from the general evolution Lemma 6 in Sec. A.3. Specifically, *strict logarithmic concavity* on the entire domain implies that the Hessian of $H(Q, P)$ can be bounded (for example in terms of their spectra) away from 0 and ∞ uniformly. Then \bar{V} and \bar{U} are uniformly bounded, and so are A and B . \square

The standard Gaussian satisfies this strict log-concavity assumption, but note that no symmetry requirement is imposed on \mathbf{g} . From the solution, observe that with a well chosen positive but small T such that $0 < T < \pi/|A|$, we have $\left| \frac{\partial Q}{\partial q} \right| = |\cos(tA)| \leq \beta < 1$.

Corollary 1. *Suppose both the target \mathfrak{f} and auxiliary \mathbf{g} are strictly log-concave, and the AD-HMC algorithm implements exact Hamiltonian dynamics for T such that $0 < T < \pi/|A|$ with $A = \sqrt{\bar{V}\bar{U}}$. Then the algorithm converges geometrically to the target \mathfrak{f} .*

4.2 Relaxed Condition on the Hessian

In this section, we will relax the uniform strictly logarithmic concave conditions over the entire space. Instead, we only require that it holds outside a compact

set. To facilitate the analysis, we assume the compact set to be, $B_R = \{q : \mathfrak{d}(q, 0) \leq R\}$, in the metric space.

Theorem 3. *If $\left| \frac{\partial Q}{\partial q} \right| \leq \beta < 1$ in $B_R^c = \{q : \mathfrak{d}(q, 0) > R\}$, and $\left| \frac{\partial Q}{\partial q} \right|$ is bounded within B_R , for some real number $R > 0$, then there exists an $\epsilon > 0$ such that the Markov recursion converges geometrically in Wasserstein metric with a rate at least $\beta' = \max\{1 - \epsilon, \frac{1+\beta}{2}\}$.*

Theorem 3 thus relaxes the strict log-concavity on \mathbf{g} , and in particular covers any auxiliary (symmetric or not) distribution that has a corresponding non-empty B_R . The proof of Theorem 3, details in Sec. A.6, relies on the following definition and two lemmas.

Definition 3. *A set C in the state space is called small (or (n_0, ϵ) -small) if there exists $n_0 \in \mathbb{Z}$ and $\epsilon > 0$, and a probability measure ν on the state space such that for any $x \in C$, $\mathbb{P}^{n_0}(x, \cdot) \geq \epsilon \nu(\cdot)$.*

Lemma 1. *B_{2R} is a small set.*

Lemma 2. *Under the conditions of Theorem 3, for $C = B_{2R}$, and for all $(q_1, q_2) \notin C \times C$,*

$$W_1(\mu(q_1), \mu(q_2)) \leq \frac{1+\beta}{2} \mathfrak{d}(q_1, q_2). \quad (4)$$

Proof of Lemmas 1 and 2 can be found in Secs. A.4 and A.5 respectively. Similar to Corollary 1, we have the following geometric convergence result.

Corollary 2. *Suppose both the target \mathfrak{f} and auxiliary \mathbf{g} are strictly log-concave outside B_R for a positive constant $R > 0$, and the AD-HMC algorithm implements exact Hamiltonian dynamics for T such that $0 < T < \pi/|A|_{B_R^c}$ with $A = \sqrt{\bar{V}\bar{U}}$. Then the algorithm converges geometrically to the target \mathfrak{f} .*

Lemmata 1 and 2 are closely related to the important concepts of (pseudo-)small set and Lyapunov function of a Markov chain. In fact, under the same conditions, (4) can be viewed as a bivariate drift condition for $\alpha := (1 + \beta)/2$ for some function $r(\cdot, \cdot)$, taking the form of the distance function, then, the results in probability theory, see, e.g. Rosenthal (2002), implies geometric convergence in total variational distance via a coupling method that inspired some of our arguments here, see, e.g. Rosenthal (2002). For more detailed information on (pseudo-)small set and Lyapunov function techniques, please see systematic treatments in Roberts and Rosenthal (2001), Roberts and Rosenthal (2004) and Meyn et al. (2009).

4.3 HMC with Numerical Integrators

In practice, HMC is implemented with numerical solutions to the Hamiltonian system of equations (1), and coupled with the well-known Metropolis-Hasting

acceptance/rejection step to ensure the convergence to the target distribution. Various numerical methods are available for this purpose, for example, the symplectic leapfrog integrator (Verlet, 1967) can be commonly seen in many literature and software implementations, and versions of the Runge-Kutta method can achieve high order of approximation. For a detailed discussion on these methods and their analysis, see, e.g. Hairer et al. (2013). More specifically, for an integer s , an approximation is of s -order if its error is $O(h^s)$ as the step size $h \rightarrow 0$. Therefore, for any real number $\delta > 0$, a proper step size can be chosen, such that the numerical method (e.g. Runge-Kutta method for high order approximation) produces $(\tilde{Q}(t), \tilde{P}(t))$ satisfying uniformly over all initial conditions that:

$$\mathfrak{d}(Q(t), \tilde{Q}(t)) + \mathfrak{d}(P(t), \tilde{P}(t)) < \delta. \quad (5)$$

Theorem 4. *If $\left| \frac{\partial Q}{\partial q} \right| \leq \beta < 1$ outside $B_R = \{q : \mathfrak{d}(q, 0) \leq R\}$ for some $R > 0$, and bounded within B_R , and condition (5) is satisfied, then the recursion generated by the numerical-approximation AD-HMC procedure converge geometrically in Wasserstein metric.*

The proof of the theorem (in Sec. A.7) adapts the same techniques as those in the above section.

5 Numerical Experiments

In this section, we study the efficacy of using an asymmetric momentum distribution $\mathfrak{g}(p)$ along with AD-HMC over using Gaussian distributions in standard HMC. Let $N(\mu, \Sigma)$ define a Gaussian with mean μ and covariance matrix Σ . We provide results for two sets of experiments for moderate dimensional targets \mathfrak{f} . The first is a simulated model where we set the target distribution of our experiments to reside in \mathbb{R}^3 , while in the second the HMC methods are applied to a Bayesian logistic regression application. Additional details and comparisons (e.g. poor performance of standard HMC with asymmetric distributions) are available in the supplementary material.

HMC methods. We include the basic HMC Algorithm (Alg. 1) with symmetric Gaussians as auxiliaries. The ‘ $N(I)$ ’ case uses $\mathfrak{g}(p) \sim N(0, I)$ to represent the standard approach. Recall that an adaptive procedure to set the Σ to the most skewed covariance, equivalent to the highest local skewness in the Hessian $\nabla^2 U(q)$ of the potential $U(q)$, is conjectured to better regularize the resulting Hamiltonian dynamics. We call this dynamically varying symmetric Gaussian auxiliary case the ‘**adapt-single**’ scheme. After every n_a iterations, the particles in iterate h_{n_a} are run through the OPTICS (Ankerst et al., 1999) clustering algorithm to classify them into distinct classes, if possible. Then, the

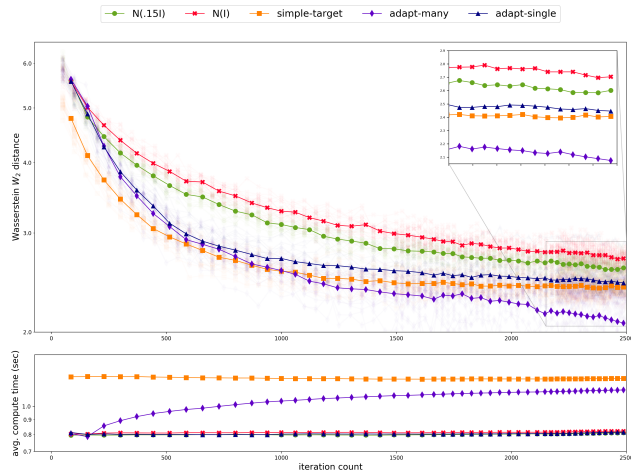


Figure 1: Performance of three HMC (‘ $N(I)$ ’, ‘ $N(.15I)$ ’ and ‘**adapt-single**’) and two AD-HMC (‘**adapt-many**’ and ‘**simple-target**’) methods: (top) W_2 distance between iterate and target distribution, and (bottom) average CPU seconds, both over iteration counts.

‘**adapt-single**’ case adopts the mean μ_c and covariance estimates Σ_c of the cluster with most skewed Σ_c as the replacement for the parameters of its Gaussian auxiliary distribution.

We consider a similar adaptive heuristic where the auxiliary is allowed to be a Gaussian mixture. Formally, the ‘**adapt-many**’ heuristic starts with $\mathfrak{g}_0(p) \sim N(0, I)$ and at each iteration $n = kn_a$, $k = 1, 2, \dots$:

1. Apply labels $c = -1, 0, \dots, C$ to all the particle samples in the current iterate h_{n_a} using the OPTICS clustering algorithm, which dynamically determines both C and the assignment of labels; the samples in the $c = -1$ class denote those that were not classified.
2. For each c , let s_c represent the number of samples in the class, and set $S = \sum_{c=0}^C s_c$. Estimate the sample mean μ_c and covariance matrix Σ_c and set $\nu_c = s_c/S$.
3. Set the auxiliary distribution $\mathfrak{g}_k(p) \sim \{N(\mu_c, \Sigma_c) \text{ w.p. } \nu_c, c = 0, \dots, C\}$.
4. Continue the AD-HMC algorithm with $\mathfrak{g}_k(p)$ for another n_a iterations.

The AD-HMC algorithm admits each auxiliary of the form constructed by ‘**adapt-many**’ and the method converges for any single such choice. While our analysis does not cover this dynamically adapting version of the auxiliary, we are actively pursuing a theory for the convergence of adaptive AD-HMC algorithms.

Simulation Model in \mathbb{R}^3 . The target \mathfrak{f} constitutes as a mixture of 12 uncorrelated gaussian densities $N(\mu, \sigma^2 I)$ with the means μ arranged so that they lie along three linearly independent lines, and standard deviations in the range $\sigma \in [0.15, 1.0]$. For this model, we add the ‘ $N(.15I)$ ’ HMC case, which sets

the auxiliary’s variance to the lowest (known) value, $g(p) \sim N(0, 0.15^2 I)$. As a reference, we also study the convergence of AD-HMC with a mixture-of-Gaussians (call it the ‘simple-target’ case) that is constructed from foreknowledge of the target as its simplification that retains six of the twelve Gaussians. The supplement provides further details on this study.

The top panel in Figure 1 plots the sample paths and averages of the three HMC and two AD-HMC cases of the Wasserstein W_2 distance between the (collection of particle samples representing the) iterate distributions h_n and the target distribution, as approximated using the Sinkhorn method Feydy et al. (2019). The top figure plots this over the iteration count, and is seen to establish the geometric convergence of the methods. A clear ordering is observed in both figures between the HMC and AD-HMC cases, with the AD-HMC cases getting closer to the target than HMC at termination. Within the HMC cases, knowledge of the lowest variance does speed convergence as anticipated. The adaptive scheme ‘adaptive-single’ performs even better than the perfect-knowledge case ‘ $N(.15I)$ ’, which may be because of the very skewed covariance estimates encountered in the earlier iterations. The perfect-knowledge asymmetric case ‘simple-target’ narrowly beats the ‘adaptive-single’ scheme in terms of iteration count. Finally, the asymmetric adaptive Gaussian mixture case ‘adaptive-many’ attains the best performance overall in both figures, and indeed continues to improve while the other algorithms have slowed down.

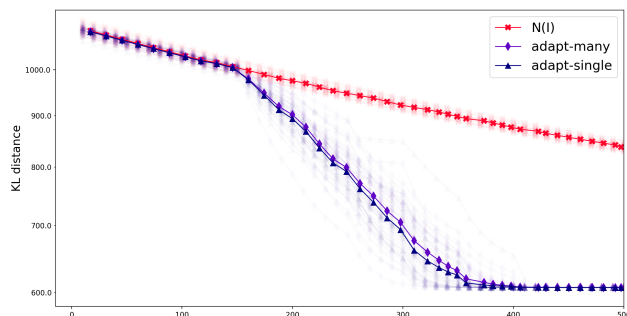


Figure 2: Performance of the HMC (‘ $N(I)$ ’ and ‘adapt-single’) and AD-HMC (‘adapt-many’) settings: Kullback-Leibler distance between iterates and the target posterior distribution over iteration counts.

Figure 1’s bottom panel provides the average CPU wallclock time per iteration for each method. The three HMC methods take the same order of effort, while the full-knowledge asymmetric distribution ‘simple-target’ takes the longest time on average since it consists of a mixture of six of the twelve Gaussians that constitute the target. The ‘adapt-many’ case takes increasing time over the iterations, reflecting the increasing complexity of the auxiliary; indeed, on average it includes five Gaussians towards the end.

Bayesian logistic regression (BLR). We study a public domain regression dataset (Huq and Cleland, 1990) that seeks to explain contraceptive use by women based on their age, number of children and urban/rural residence. The target Bayesian posterior density over \mathbb{R}^4 is given by $f(q) \propto \pi(q)P(x|q)$, where $\pi(q)$ is the prior distribution and $P(x|q)$ represents the likelihood of observed data x given regression coefficient q . The supplement provides full details on this model. Figure 2 plots the sample paths and averages of the two HMC methods ‘ $N(I)$ ’ and ‘adaptive-single’, and the AD-HMC case ‘adaptive-many’. Since the exact target is unavailable, we measure their performance using the Kullback-Leibler divergence from the posterior, as is the standard in variational inference algorithms. The two adaptive schemes produce markedly faster convergence over standard HMC, indeed seeming to have converged, while the ‘ $N(I)$ ’ slowly approaches the solution. The iterations tend to concentrate the posterior’s mass around a mean regression parameter value as expected for logistic regression, and this unimodal nature of the target limits the advantage of ‘adaptive-many’ over ‘adaptive-single’.

Parameter Settings. All algorithms were implemented in python 3.7 and ran on a server with two AMD EPYC 7301 16-core processors and 64Gb system memory and two GeForce RTX2070 8Gb GPUs. The iterate distribution h_n is represented by empirical distributions with 900 samples. AD-HMC sample paths are run for 2500 and 500 iterations respectively for the simulation and BLR model, and for a fair comparison the HMC paths are allowed double the number of iterations. The adaptive methods set $n_a = 150$, and the averages are developed from 20 sample paths. The Hamiltonian motion dynamics in both algorithms are approximated by the leapfrog symplectic numerical integration procedure (Verlet, 1967); see Supplement section B. Each iteration takes L discrete first-order approximation steps of size ϵ to implement Hamiltonian motion of length $T = L\epsilon$, with (L, ϵ) of $(100, 0.025)$ in simulated dataset and $(50, 0.00025)$ for the BLR model. The OPTICS clustering scheme is run with its default parameters in the Scipy library (Pedregosa et al., 2011). Note that the clustering step limits the use of the adaptive schemes to only moderate dimensional settings.

Summary. The numerical evidence shows that the AD-HMC based ‘adapt-many’, a straightforward heuristic to model the auxiliary distribution on key characteristics of the target distribution, can notably speed up estimation of the target distribution over plain HMC. This shows a promising avenue for further exploration both in practical adaptive auxiliary design algorithms and in rigorously understanding when they may converge faster.

Societal Impact

This is a theoretical contribution that, nevertheless, has the potential of impacting a wide range of application domains in business, engineering and science. In particular, all of those in which Hamiltonian Monte Carlo methods have been used as a statistical inference and estimation tool (e.g. image analysis and computer vision, signal processing, operations research, and so on). Because our paper provides a step towards generalizing and relaxing the conditions needed on the method's parameters in order to establish statistical rates of convergence, we believe that we have the potential of speeding up and thus enabling more applications.

References

- C. Andrieu, N. D. Freitas, A. Doucet, and M. I. Jordan. An introduction to mcmc for machine learning. machine learning. *Machine Learning*, 50:5–43, 2003.
- M. Ankerst, M. M. Breunig, H.-P. Kriegel, and J. Sander. Optics: Ordering points to identify the clustering structure. *SIGMOD Rec.*, 28(2):49–60, June 1999. ISSN 0163-5808. doi: 10.1145/304181.304187. URL <https://doi.org/10.1145/304181.304187>.
- M. Betancourt, S. Byrne, S. Livingstone, and M. Girolami. The geometric foundations of hamiltonian monte carlo. *Bernoulli*, 23(4A):2257–2298, 11 2017. doi: 10.3150/16-BEJ810. URL <https://doi.org/10.3150/16-BEJ810>.
- V. Bogachev. *Measure Theory*. Number v. 1 in Measure Theory. Springer Berlin Heidelberg, 2007. ISBN 9783540345145. URL <https://books.google.com/books?id=CoSIE7h5mTsC>.
- N. Bou-Rabee and J. M. Sanz-Serna. Randomized hamiltonian monte carlo. *Ann. Appl. Probab.*, 27(4):2159–2194, 08 2017. doi: 10.1214/16-AAP1255. URL <https://doi.org/10.1214/16-AAP1255>.
- N. Bou-Rabee, A. Eberle, and R. Zimmer. Coupling and convergence for hamiltonian monte carlo. *Ann. Appl. Probab.*, 30(3):1209–1250, 06 2020. doi: 10.1214/19-AAP1528. URL <https://doi.org/10.1214/19-AAP1528>.
- B. Carpenter, A. Gelman, M. Hoffman, D. Lee, B. Goodrich, M. Betancourt, M. Brubaker, J. Guo, P. Li, and A. Riddell. Stan: A probabilistic programming language. *Journal of Statistical Software, Articles*, 76(1):1–32, 2017. ISSN 1548-7660. doi: 10.18637/jss.v076.i01. URL <https://www.jstatsoft.org/v076/i01>.
- M.-F. Chen. Equivalence of exponential ergodicity and l2-exponential convergence for markov chains. *Stochastic Processes and their Applications*, 87(2):281 – 297, 2000. ISSN 0304-4149. doi: [https://doi.org/10.1016/S0304-4149\(99\)00114-3](https://doi.org/10.1016/S0304-4149(99)00114-3). URL <http://www.sciencedirect.com/science/article/pii/S0304414999001143>.
- Z. Chen and S. S. Vempala. Optimal convergence rate of hamiltonian monte carlo for strongly logconcave distributions. *RANDOM*, 2019.
- S. Duane, A. Kennedy, B. J. Pendleton, and D. Roweth. Hybrid monte carlo. *Physics Letters B*, 195(2):216 – 222, 1987. ISSN 0370-2693. doi: [https://doi.org/10.1016/0370-2693\(87\)91197-X](https://doi.org/10.1016/0370-2693(87)91197-X). URL <http://www.sciencedirect.com/science/article/pii/037026938791197X>.
- A. Durmus and É. Moulines. Quantitative bounds of convergence for geometrically ergodic markov chain in the wasserstein distance with application to the metropolis adjusted langevin algorithm. *Statistics and Computing*, 25(1):5–19, 2015. doi: 10.1007/s11222-014-9511-z. URL <https://doi.org/10.1007/s11222-014-9511-z>.
- A. Durmus, É. Moulines, and E. Saksman. On the convergence of hamiltonian monte carlo. *arXiv: Computation*, 2017.
- J. Feydy, T. Séjourné, F.-X. Vialard, S.-i. Amari, A. Trounev, and G. Peyré. Interpolating between optimal transport and mmd using sinkhorn divergences. In *The 22nd International Conference on Artificial Intelligence and Statistics*, pages 2681–2690, 2019.
- A. E. Gelfand and A. F. M. Smith. Sampling-based approaches to calculating marginal densities. *Journal of the American Statistical Association*, 85(410):398–409, 1990. doi: 10.1080/01621459.1990.10476213.
- A. Gelman, J. B. Carlin, H. S. Stern, D. B. Dunson, A. Vehtari, and D. B. Rubin. *Bayesian Data Analysis*. Chapman and Hall/CRC, 2013.
- M. Girolami and B. Calderhead. Riemann manifold langevin and hamiltonian monte carlo methods. *Journal of the Royal Statistical Society: Series B (Statistical Methodology)*, 73(2):123–214, 2011. doi: 10.1111/j.1467-9868.2010.00765.x. URL <https://rss.onlinelibrary.wiley.com/doi/abs/10.1111/j.1467-9868.2010.00765.x>.
- E. Hairer, C. Lubich, and G. Wanner. *Geometric Numerical Integration: Structure-Preserving Algorithms for Ordinary Differential Equations*. Springer Series in Computational Mathematics. Springer Berlin Heidelberg, 2013. ISBN 9783662050187. URL <https://books.google.com/books?id=cPTxCAAQBAJ>.
- M. Hairer, J. C. Mattingly, and M. Scheutzow. Asymptotic coupling and a general form of harris’ theorem

- with applications to stochastic delay equations. *Probability Theory and Related Fields*, 149(1):223–259, 2011. doi: 10.1007/s00440-009-0250-6. URL <https://doi.org/10.1007/s00440-009-0250-6>.
- W. K. Hastings. Monte carlo sampling methods using markov chains and their applications. *Biometrika*, 57(1):97–109, 1970. ISSN 00063444. URL <http://www.jstor.org/stable/2334940>.
- N. M. Huq and J. Cleland. Bangladesh fertility survey 1989 (main report). Technical report, Dhaka: National Institute of Population Research and Training, 1990.
- J. Jasche and F.-S. Kitaura. Fast hamiltonian sampling for large-scale structure inference. *Monthly Notices of the Royal Astronomical Society*, 407:29 – 42, 09 2010. doi: 10.1111/j.1365-2966.2010.16897.x.
- A. Joulin and Y. Ollivier. Curvature, concentration and error estimates for markov chain monte carlo. *Ann. Probab.*, 38(6):2418–2442, 11 2010. doi: 10.1214/10-AOP541. URL <https://doi.org/10.1214/10-AOP541>.
- B. Leimkuhler and S. Reich. *Simulating Hamiltonian Dynamics*. Cambridge Monographs on Applied and Computational Mathematics. Cambridge University Press, 2004. ISBN 9780521772907. URL <https://books.google.com/books?id=tpb-tnsZi5YC>.
- T. Lelievre, M. Rousset, and G. Stoltz. Langevin dynamics with constraints and computation of free energy differences, 2010.
- S. Livingstone, M. Betancourt, S. Byrne, and M. Girolami. On the geometric ergodicity of hamiltonian monte carlo. *Bernoulli*, 25(4A):3109–3138, 11 2019. doi: 10.3150/18-BEJ1083. URL <https://doi.org/10.3150/18-BEJ1083>.
- O. Mangoubi and A. Smith. Rapid mixing of hamiltonian monte carlo on strongly log-concave distributions. *Proceedings of Machine Learning Research*, 89, 2019.
- P. A. Markowich and C. Villani. On the trend to equilibrium for the fokker-planck equation: An interplay between physics and functional analysis. *Matematica Contemporanea (SBM)*, 19:1–31, 2000.
- S. Meyn, R. Tweedie, and P. Glynn. *Markov Chains and Stochastic Stability*. Cambridge Mathematical Library. Cambridge University Press, 2009. ISBN 9780521731829. URL <https://books.google.com/books?id=Md7RnYEPkJwC>.
- R. M. Neal. Bayesian learning via stochastic dynamics. In S. J. Hanson, J. D. Cowan, and C. L. Giles, editors, *Advances in Neural Information Processing Systems 5*, pages 475–482. Morgan-Kaufmann, 1993.
- Y. Ollivier. Ricci curvature of markov chains on metric spaces. *Journal of Functional Analysis*, 256(3):810 – 864, 2009. ISSN 0022-1236. doi: <https://doi.org/10.1016/j.jfa.2008.11.001>. URL <http://www.sciencedirect.com/science/article/pii/S002212360800493X>.
- F. Pedregosa, G. Varoquaux, A. Gramfort, V. Michel, B. Thirion, O. Grisel, M. Blondel, P. Prettenhofer, R. Weiss, V. Dubourg, J. Vanderplas, A. Passos, D. Cournapeau, M. Brucher, M. Perrot, and E. Duchesnay. Scikit-learn: Machine learning in Python. *Journal of Machine Learning Research*, 12:2825–2830, 2011.
- C. Robert and G. Casella. *Monte Carlo Statistical Methods*. Springer, 2004.
- G. O. Roberts and J. S. Rosenthal. Small and pseudo-small sets for markov chains. *Stochastic Models*, 17(2):121–145, 2001. doi: 10.1081/STM-100002060. URL <https://doi.org/10.1081/STM-100002060>.
- G. O. Roberts and J. S. Rosenthal. General state space markov chains and mcmc algorithms. *Probab. Surveys*, 1:20–71, 2004. doi: 10.1214/154957804100000024. URL <https://doi.org/10.1214/154957804100000024>.
- J. Rosenthal. Quantitative convergence rates of markov chains: A simple account. *Electron. Commun. Probab.*, 7:123–128, 2002. doi: 10.1214/ECP.v7-1054. URL <https://doi.org/10.1214/ECP.v7-1054>.
- A. M. Stuart. Inverse problems: A bayesian perspective. *Acta Numerica*, 19:451–559, 2010. doi: 10.1017/S0962492910000061.
- M. Talagrand. Transportation cost for gaussian and other product measures. *Geometric & Functional Analysis GFA*, 6(3):587–600, May 1996. ISSN 1420-8970. doi: 10.1007/BF02249265. URL <https://doi.org/10.1007/BF02249265>.
- S. D. Team. Stan modeling language users guide and reference manual, 2017. URL <https://mc-stan.org/>.
- L. Verlet. Computer "experiments" on classical fluids. i. thermodynamical properties of lennard-jones molecules. *Phys. Rev.*, 159:98–103, Jul 1967. doi: 10.1103/PhysRev.159.98. URL <https://link.aps.org/doi/10.1103/PhysRev.159.98>.
- C. Villani. *Optimal Transport: Old and New*. Grundlehren der mathematischen Wissenschaften. Springer Berlin Heidelberg, 2008. ISBN 9783540710509. URL https://books.google.com/books?id=hV8o5R7_5tkC.

SUPPLEMENTARY MATERIAL

A Proofs

A.1 Proof of Theorem 1

We assume the operator \mathcal{T} is self-adjoint, and has invariance and coverage properties. All the arguments applies also to the operator \mathcal{T}_a which is self-adjoint as $\mathcal{T}_a^\dagger = (\mathcal{T} \circ \mathcal{T}^\dagger)^\dagger = (\mathcal{T}^\dagger)^\dagger \circ \mathcal{T}^\dagger = \mathcal{T} \circ \mathcal{T}^\dagger = \mathcal{T}_a$ and inherits the invariance properties as well.

Lemma 3. $\mathcal{T}h = \int_{\mathbb{P}}(h/f) \circ \mathcal{R} \cdot \mathbf{g}$ is an averaging operator, and $\mathcal{T}\mathbf{f} = \mathbf{f}$ is a fixed point.

Proof. By the invariance property, $\mathcal{T}h = \int_{\mathbb{P}}(h/f) \circ \mathcal{R} \cdot (\mathbf{f} \cdot \mathbf{g}) \circ \mathcal{R} = \int_{\mathbb{P}}(h/f) \circ \mathcal{R} \cdot \mathbf{f} \cdot \mathbf{g} = \mathbf{f} \int_{\mathbb{P}}(h/f) \circ \mathcal{R} \cdot \mathbf{g}$. That shows that any h proportional to \mathbf{f} is a fixed point of \mathcal{T} . \square

Lemma 4. The operator \mathcal{T} is well defined on the non-empty $L_{\mathbf{f}}^2 \ni \mathbf{f}$. It strictly decreases the norm $\|\mathcal{T}h\| < \|h\|$ unless $h = \text{const} \cdot \mathbf{f}$ in which case it is a fixed point of the operator.

Proof. We have $\|\mathbf{f}\|^2 = \int_{\mathbb{Q}}(\mathbf{f})^2/\mathbf{f} = \int_{\mathbb{Q}}\mathbf{f} < \infty$.

$$\begin{aligned} \|\mathcal{T}h\|^2 &= \int_{\mathbb{Q}} \frac{(\mathbf{f} \int_{\mathbb{P}}(h/f) \circ \mathcal{R} \cdot \mathbf{g})^2}{\mathbf{f}} \leq \iint_{\mathbb{Q} \times \mathbb{P}} \left(\frac{h}{\mathbf{f}} \circ \mathcal{R} \right)^2 \cdot (\mathbf{g} \cdot \mathbf{f}) = \iint_{\mathbb{Q} \times \mathbb{P}} \left(\frac{h}{\mathbf{f}} \circ \mathcal{R} \right)^2 \cdot (\mathbf{g} \cdot \mathbf{f}) \circ \mathcal{R} \\ &= \iint_{\mathbb{Q} \times \mathbb{P}} \left(\frac{h}{\mathbf{f}} \right)^2 \cdot (\mathbf{g} \cdot \mathbf{f}) = \left(\int_{\mathbb{Q}} \frac{h^2}{\mathbf{f}} \right) \cdot \left(\int_{\mathbb{P}} \mathbf{g} \right) = \|h\|^2 \cdot 1 \end{aligned}$$

The equality happens only if for \mathbf{f} -a.e. q we have $(\int_{\mathbb{P}}(h/f) \circ \mathcal{R} \cdot \mathbf{g})^2 = \int_{\mathbb{P}}(h/f)^2 \circ \mathcal{R} \cdot \mathbf{g}$, but for that $(h/f) \circ \mathcal{R} = (h/f)(Q(q, p))$ must be constant with respect to \mathbf{g} -a.e. p . The coverage assumption forces the constant to be the same for (almost surely) all q . It follows that either $h = \alpha \mathbf{f} = \mathcal{T}h$ with equal norms or otherwise the norm is strictly decreasing, i.e. $\|\mathcal{T}h\|^2 < \|h\|^2$. \square

Lemma 5. The operator \mathcal{T} conserves the integral $\int_{\mathbb{Q}} \mathcal{T}h = \int_{\mathbb{Q}} h = \langle \mathbf{f}, h \rangle$.

Proof. By the invariance property, $\int_{\mathbb{Q}} \mathcal{T}h = \iint_{\mathbb{Q} \times \mathbb{P}} (h \circ \mathbf{g}) \circ \mathcal{R} = \iint_{\mathbb{Q} \times \mathbb{P}} (h \circ \mathbf{g}) = (\int_{\mathbb{Q}} h) \cdot (\int_{\mathbb{P}} \mathbf{g}) = \int_{\mathbb{Q}} h \cdot 1$. The last statement follows from the definition of the scalar product in L^2 space. \square

Lemma 4 allows us to define $S(h) = \lim_{n \rightarrow \infty} \|\mathcal{T}^n h\|^2 = \inf_n \|\mathcal{T}^n h\|^2$. Clearly for any M we have $S(h) = S(\mathcal{T}^M h)$. Next, a crucial proposition is established utilizing self-adjointness.

Proposition 2. Any weak accumulation point h_∞ of the sequence $\mathcal{T}^n h$ satisfies $\|h_\infty\|^2 = S(h)$.

Proof. By the definition of weak convergence $\mathcal{T}^{n_k} h \rightharpoonup h_\infty$ for a subsequence \mathcal{T}^{n_k} , we have $\langle \mathcal{T}^{n_k} h, a \rangle \rightarrow \langle h_\infty, a \rangle$ for any $a \in L^2$. In particular $\int h = \int \mathcal{T}^{n_k} h = \langle \mathcal{T}^{n_k} h, \mathbf{f} \rangle \rightarrow \langle h_\infty, \mathbf{f} \rangle = \int h_\infty$, where we use Lemma 5. We can assume that given an $\epsilon > 0$ we have $S(h) \leq \|h\|^2 \leq S(h) + \epsilon$ and that the subsequence contains infinitely many even iterates \mathcal{T}^{2m} , otherwise take some $M > 0$ and use $\mathcal{T}^M h$ in place of h . We now use self-adjointness: $S(h) \leq \|\mathcal{T}^m h\|^2 = \langle \mathcal{T}^m h, \mathcal{T}^m h \rangle = \langle \mathcal{T}^{2m} h, h \rangle \rightarrow \langle h_\infty, h \rangle \leq \|h_\infty\| \cdot \|h\| \leq \|h_\infty\| \cdot (S(h) + \epsilon)^{1/2}$. That proves $\|h_\infty\| \geq S(h)^{1/2}$. The opposite inequality is standard $\|h_\infty\|^2 \leftarrow \langle \mathcal{T}^{n_k} h, h_\infty \rangle \leq \|\mathcal{T}^{n_k} h\| \cdot \|h_\infty\|$. \square

Corollary 3. The sequence $\mathcal{T}^n h$ converges weakly to $\alpha \mathbf{f}$, with $\alpha = \int h / \int \mathbf{f}$.

Proof. If $\mathcal{T}^{n_k} h \rightharpoonup h_\infty$ then $\mathcal{T}^{n_k+1} h \rightharpoonup \mathcal{T}h_\infty$ and both have the same norm $S(h)^{1/2}$. But it is possible only if $h_\infty = \alpha \mathbf{f} = \mathcal{T}h_\infty$, and $\int h = \int h_\infty = \alpha \int \mathbf{f}$. Hence all weakly convergent subsequences of $\mathcal{T}^n h$ have the same limit, and as in L^2 every bounded sequence has a weakly converging subsequence, the whole sequence $\mathcal{T}^n h$ converges weakly to $\alpha \mathbf{f}$. \square

Proposition 3. *The sequence $\mathcal{T}^n h$ converges strongly:*

$$\left\| \mathcal{T}^n h - \frac{\int_{\mathbb{Q}} h}{\int_{\mathbb{Q}} \mathfrak{f}} \cdot \mathfrak{f} \right\| \rightarrow 0.$$

Proof. By Corollary 3, $\mathcal{T}^n h \rightharpoonup h_\infty = \alpha \mathfrak{f}$. The strong convergence follows from the weak convergence and the convergence of norms to the norm of the limit $\|\mathcal{T}^n h - h_\infty\|^2 = \|\mathcal{T}^n\|^2 - 2\langle \mathcal{T}^n h, h_\infty \rangle + \|\alpha \mathfrak{f}\|^2 \rightarrow \mathcal{S}(h) - 2\langle h_\infty, h_\infty \rangle + \|h_\infty\|^2 = \mathcal{S}(h) - \|h_\infty\|^2 = 0$. \square

A.2 Proof of Theorem 2

Proof. Recall that to bound κ away from zero, we will need to provide a uniform (and ≤ 1) upper bound to the quantity $\frac{W_1(\mu(q_1), \mu(q_2))}{\mathfrak{d}(q_1, q_2)}$ for any pair of q_1 and q_2 . This upper bound will be achieved by two relaxations. First, we identify one member γ_0 in the set of joint distributions $\Gamma(\mu(q_1), \mu(q_2))$. By definition 1, the integration, $\int_{\mathbb{Q} \times \mathbb{Q}} \mathfrak{d}(x, y) \gamma_0(dx, dy)$, naturally provides an upper bound to $W_1(\mu(q_1), \mu(q_2))$. The second relaxation is on the calculation of the function $\mathfrak{d}(x, y)$ within the integration $\int_{\mathbb{Q} \times \mathbb{Q}} \mathfrak{d}(x, y) \gamma_0(dx, dy)$.

The basic idea of the first relaxation is the same as that of the common random number generator in simulation literature. M. Talagrand Talagrand (1996), who attributed the idea to M. Frechet, used it to prove some version of the logarithmic Sobolev inequalities, which is closely related to the geometric convergence of Markov chains.

Suppose that μ is the selected auxiliary distribution on \mathbb{P} . Define a map $\mathcal{L} : \mathbb{P} \rightarrow \mathbb{Q} \times \mathbb{Q}$ with $p \mapsto (Q(q_1, p), Q(q_2, p))$, for any given $(q_1, q_2) \in \mathbb{Q} \times \mathbb{Q}$. \mathcal{L} thus induced a measure on $\mathbb{Q} \times \mathbb{Q}$, γ_μ (can be viewed as $\mathcal{L}_\# \mu$). More specifically, for any subset $A, B \subset \mathbb{Q}$, the measure γ_μ has the following representation,

$$\gamma_\mu(A \times B) = \int_{A \tilde{\times} B} \mathfrak{g}(p) dp,$$

with $A \tilde{\times} B := \{p \in \mathbb{P}, Q(q_1, p) \in A \text{ and } Q(q_2, p) \in B\}$. it can be easily verified that $\gamma_\mu \in \Gamma(\mu(q_1), \mu(q_2))$. Therefore,

$$W_1(\mu(q_1), \mu(q_2)) \leq \int \int \mathfrak{d}(x, y) \gamma_\mu(dx, dy).$$

Naturally, it can be seen that we are coupling the two motions with the same momentum generated from the common distribution μ on \mathbb{P} .

For any subset $A, B \subset \mathbb{Q}$, the measure Γ_μ is defined as

$$\Gamma_\mu(A \times B) = \int_{A \tilde{\times} B} \mathfrak{g}(p) dp,$$

with $A \tilde{\times} B := \{p \in \mathbb{P}, Q(q_1, p) \in A \text{ and } Q(q_2, p) \in B\}$. From the property of integrability for push-forward measure, see, e.g. Bogachev (2007), we know that,

$$\int \int \mathfrak{d}(x, y) \Gamma_\mu(dx, dy) = \int \mathfrak{d}(Q(q_1, p), Q(q_2, p)) \mathfrak{g}(p) dp$$

For the second relaxation, the quantity $\mathfrak{d}(Q(q_1, p), Q(q_2, p))$ in the above integration can be further upper bounded by the length of one specific curve that connects $Q(q_1, p)$ and $Q(q_2, p)$. More specifically, for any $t \in [0, 1] \rightarrow \mathbb{Q}$, let $\eta(t) = Q(tq_2 + (1-t)q_1, p)$. Thus, $\dot{\eta}(t) = \frac{\partial Q}{\partial q} \cdot (q_2 - q_1)$. Hence,

$$\mathfrak{d}(Q(q_1, p), Q(q_2, p)) \leq \int_0^1 \sqrt{|\dot{\eta}(t)|^2} dt \leq \left| \frac{\partial Q}{\partial q} \right| |q_2 - q_1|.$$

\square

A.3 Evolution of the dependence on the initial configuration

Lemma 6 (Evolution of the dependence on the initial configuration). *When the Hamiltonian is given by $H(Q, P) = U(Q) + V(P)$, the derivative of the motion (Q, P) with respect to the starting configuration (q, p) satisfy the following time evolution equation:*

$$\frac{\partial}{\partial t} \begin{pmatrix} \frac{\partial Q}{\partial q} & \frac{\partial Q}{\partial p} \\ \frac{\partial P}{\partial q} & \frac{\partial P}{\partial p} \end{pmatrix} = \begin{pmatrix} 0 & V'' \\ -U'' & 0 \end{pmatrix} \cdot \begin{pmatrix} \frac{\partial Q}{\partial q} & \frac{\partial Q}{\partial p} \\ \frac{\partial P}{\partial q} & \frac{\partial P}{\partial p} \end{pmatrix} \quad (6)$$

with initial condition,

$$\begin{pmatrix} \frac{\partial Q}{\partial q} & \frac{\partial Q}{\partial p} \\ \frac{\partial P}{\partial q} & \frac{\partial P}{\partial p} \end{pmatrix}_{t=0} = \begin{pmatrix} I & 0 \\ 0 & I \end{pmatrix} \quad (7)$$

Proof. By continuity of derivatives we can exchange their order, for instance:

$$\frac{\partial}{\partial t} \left(\frac{\partial Q}{\partial q} \right) = \frac{\partial \dot{Q}}{\partial q} = \frac{\partial}{\partial q} \frac{\partial H}{\partial P} = \frac{\partial^2 H}{\partial Q \partial P} \cdot \frac{\partial Q}{\partial q} + \frac{\partial^2 H}{\partial P^2} \cdot \frac{\partial P}{\partial q} = 0 \cdot \frac{\partial Q}{\partial q} + \frac{\partial^2 H}{\partial P^2} \cdot \frac{\partial P}{\partial q} = V'' \cdot \frac{\partial P}{\partial q}.$$

The remaining derivatives are calculated in the similar way. Furthermore, when we integrate the differential equation (1), we obtain:

$$\begin{aligned} Q(t) &= q + \int_0^t (\partial \mathcal{H}(Q(s), P(s)) / \partial P) ds \\ P(t) &= p - \int_0^t (\partial \mathcal{H}(Q(s), P(s)) / \partial Q) ds, \end{aligned} \quad (8)$$

and the initial condition can be easily deduced from that (8), the formal representation of the solution. \square

For symmetric, positive definite operators on L^2 , U and V , their symmetric positive definite square roots are uniquely defined. For example, for $V < I$ (that is $I - V$ is positive definite, which can be achieved by a normalization trick) $\sqrt{V} = I - R$ where R is a limit of the (strongly converging) sequence $R_{n+1} = (I - (V - R_n^2)) / 2$, $R_0 = 0$. Also VU and UV are positive definite (but not necessarily symmetric, when non commuting), as for example $VU = \sqrt{U}^{-1} (\sqrt{UV} \sqrt{U}) \sqrt{U}$ is similar via a symmetric operator \sqrt{U} to a symmetric positive definite $\sqrt{UV} \sqrt{U}$. Using this we can define $\sqrt{VU} = \sqrt{U}^{-1} \sqrt{\sqrt{UV} \sqrt{U}} \sqrt{U}$, and similarly \sqrt{UV} .

Below the functions are defined by their power series $\exp(x) = \sum_{n=0}^{\infty} x^n / n!$, $\sin(x) = \sum_{n=0}^{\infty} (-1)^n x^{2n+1} / (2n+1)!$, $\text{sinc}(x) = x^{-1} \sin(x) = \sum_{n=0}^{\infty} (-1)^n x^{2n} / (2n+1)!$, which is well defined even when x^{-1} is not and $\cos(x) = \sum_{n=0}^{\infty} (-1)^n x^{2n} / (2n)!$.

Lemma 7 (Exponential function of a matrix). *Let V, U be symmetric, positive definite linear operators in L^2 . If for $t \in \mathbb{R}$*

$$\mathcal{C} = \begin{pmatrix} 0 & tV \\ -tU & 0 \end{pmatrix}$$

then for $A = \sqrt{VU}$ and $B = \sqrt{UV}$ we have

$$\exp(\mathcal{C}) = \sum_{n=0}^{\infty} (-1)^n \mathcal{C}^n = \begin{pmatrix} \cos(tA) & tV \text{sinc}(tB) \\ -tU \text{sinc}(tA) & \cos(tB) \end{pmatrix}.$$

Proof. From direct calculation of \mathcal{C}^2 we have the following powers of \mathcal{C} :

$$\begin{aligned} \mathcal{C}^{2n} &= (-1)^n \begin{pmatrix} (VU)^n t^{2n} & 0 \\ 0 & (UV)^n t^{2n} \end{pmatrix} = (-1)^n \begin{pmatrix} (At)^{2n} & 0 \\ 0 & (Bt)^{2n} \end{pmatrix}; \\ \mathcal{C}^{2n+1} &= (-1)^n \begin{pmatrix} 0 & V(UV)^n t^{2n+1} \\ -U(VU)^n t^{2n+1} & 0 \end{pmatrix} = (-1)^n \begin{pmatrix} 0 & tV(Bt)^{-1} (Bt)^{2n+1} \\ -tU(At)^{-1} (At)^{2n+1} & 0 \end{pmatrix}, \end{aligned}$$

so that:

$$\exp(\mathcal{C}) = \sum_{n=0}^{\infty} (-1)^n \begin{pmatrix} \frac{(tA)^{2n}}{(2n)!} & tV(tB)^{-1} \frac{(tB)^{2n+1}}{(2n+1)!} \\ -tU(tA)^{-1} \frac{(tA)^{2n+1}}{(2n+1)!} & \frac{(tB)^{2n}}{(2n)!} \end{pmatrix} = \begin{pmatrix} \cos(tA) & tV \operatorname{sinc}(tB) \\ -tU \operatorname{sinc}(tA) & \cos(tB) \end{pmatrix}.$$

We need to use the additional U and V to compensate for odd powers on the off-diagonal. \square

A.4 Proof of Lemma 1

Proof. To show that B_R is a small set, we need to construct a probability measure γ on the state space, such that $\mathbb{P}(x, A) \geq \epsilon \gamma(A)$ for any Borel set A . Suppose that for any $q \in B_R$, there exists a $\rho(q) > 0$, such that there exist a measure γ_q and an $\epsilon_q > 0$ and that $\mathbb{P}(x, A) \geq \epsilon_q \gamma_q(A)$ for any $x \in B_{\rho(q)}(q)$. Then by the compactness of B_R it can be covered by a finite number of them, $B_{\rho(q_1)}, B_{\rho(q_2)}, \dots, B_{\rho(q_N)}$, and this will imply that B_R is small.

So now, we only need to construct γ_q locally. For each q , consider the density function $\mathbb{P}(x, dy)$, for $x \in B_{\rho(q)}(q)$ for some small $\rho(q) > 0$, and any y . From the push forward definition of the transition probability, we can see that, $\mathbb{P}(x, dy) = \mathbf{g}(y - x) dp$ where $\mathbf{g}(\cdot)$ denotes the density function of the auxiliary distribution. Hence, there exists an x_0 (might be outside $B_{\rho(q)}(q)$), such that $\mathbf{g}(y - x) \geq \epsilon_q \mathbf{g}(y - x_0)$ with some $\epsilon_q \in (0, 1)$. This comes from the monotonicity of auxiliary function. In fact, we just need the monotonicity for the ease of argument, we don't believe that this is essential. \square

A.5 Proof of Lemma 2

Proof. For the bivariate drift condition, we see that it is easy to verify for $(q_1, q_2) \in C^c \times C^c$. More precisely, we know that,

$$\begin{aligned} \mathfrak{d}(Q(q_1, p), Q(q_2, p)) &\leq \int_0^1 \sqrt{|\dot{\eta}(t)|^2} dt = \int_0^1 \sqrt{\left| \frac{\partial Q(t)}{\partial q} (q_2 - q_1) \right|^2} dt \\ &= \left[\left(\int_{[0,1] \cup S: Q(t) \in C} + \int_{[0,1] \cup S: Q(t) \in C^c} \right) \sqrt{\left| \frac{\partial Q(t)}{\partial q} \right|^2} dt \right] \mathfrak{d}(q_1, q_2) \\ &\leq \left[\int_{[0,1] \cup S: Q(t) \in C} dt + \int_{[0,1] \cup S: Q(t) \in C^c} \beta dt \right] \mathfrak{d}(q_1, q_2) \leq \left[1 - \frac{2}{3}(1 - \beta) \right] \mathfrak{d}(q_1, q_2), \end{aligned}$$

the last inequality comes from the fact that any path connecting q_1, q_2 will have at least two third of it lying in the domain where $\left| \frac{\partial Q}{\partial q} \right| \leq \beta$. Next, let us consider the case of $(q_1, q_2) \in C \times C^c$, or equivalently $(q_1, q_2) \in C^c \times C$. Again, we have, similarly,

$$\mathfrak{d}(Q(q_1, p), Q(q_2, p)) \leq \left[\int_{[0,1] \cup S: Q(t) \in C} dt + \int_{[0,1] \cup S: Q(t) \in C^c} \beta dt \right] \mathfrak{d}(q_1, q_2)$$

Let $C = B_{2R}$, then for $(q_1, q_2) \in C \times C^c$, in the above integration, at least in half length of the curve, we will have $\frac{\partial Q}{\partial q} < \beta$, and the rest of length it is bounded by 1. Therefore, we have,

$$\mathfrak{d}(Q(q_1, p), Q(q_2, p)) \leq \frac{1 + \beta}{2} \mathfrak{d}(q_1, q_2),$$

and we get the required bivariate drift bound. \square

A.6 Proof of Theorem 3

Proof. This proof will again make use of the coarse Ricci curvature arguments. Recall that, we need to show that for any pair (q_1, q_2) , $W_1(\mu(q_1), \mu(q_2)) \leq \beta' \mathfrak{d}(q_1, q_2)$. We need to discuss two different cases. First, for the case of $(q_1, q_2) \notin C \times C$, from Lemma 2, we have, $W_1(\mu(q_1), \mu(q_2)) \leq \frac{1+\beta}{2} \mathfrak{d}(q_1, q_2)$. Second, for the case of $(q_1, q_2) \in C \times C$, define a joint distribution $\hat{\gamma}$ as follows. Let ξ be an independent uniform distribution in $[0, 1]$. When $\xi \leq \epsilon$, $\hat{\gamma}(\mu(q_1), \mu(q_2)) = \gamma_\nu(Q_1 \in dy, Q_2 \in dz) = \nu(Q_1(q_1, y) | Q_1(q_1, y) = Q_2(q_2, z))$, i.e. Q_1 and Q_2 will

be at the same position, which distributes according to the probability distribution ν ; when $\xi > \epsilon$, each one will be going to be $\hat{\gamma}(\mu(q_1), \mu(q_2)) = \tilde{\gamma}(\mu(q_1), \mu(q_2)) - \gamma_\nu(\mu(q_1), \mu(q_2))$. The nonnegativity of $\hat{\gamma}(\mu(q_1), \mu(q_2))$ is guaranteed by the smallness of B_R . Furthermore, it is easy to verify that the marginal distributions will not change, hence, $\hat{\gamma} \in \Gamma(\mu(q_1), \mu(q_2))$. Meanwhile, we can see that $\int \int \mathfrak{d}(x, y) \hat{\gamma}(\mu(q_1), \mu(q_2)) \leq (1 - \epsilon) \mathfrak{d}(q_1, q_2)$ because the probability that $\mathfrak{d}(\mu(q_1), \mu(q_2)) = 0$ is at least ϵ . This leads to $W_1(\mu(q_1), \mu(q_2)) \leq (1 - \epsilon) \mathfrak{d}(q_1, q_2)$. The desired estimation of the Coarse Ricci curvature follows from these two cases. \square

A.7 Proof of Theorem 4

Proof. The proof will follow the same idea as that of Theorem 3, and we show that for any pair (q_1, q_2) , $W_1(\mu(q_1), \mu(q_2)) \leq \beta' \mathfrak{d}(q_1, q_2)$. It is very easy to see that arguments for small set, i.e. Lemma 1, still go through with the condition (5) holds. The contraction of the Wasserstein distance for $(q_1, q_2) \in C \times C$ also follows with a smaller perturbation in the selection of the parameter.

Now, let us look at bivariate drift condition. For any $(q_1, q_2) \notin C \times C$, for any $p \in \mathbb{P}$, recall that the exact solutions to the Hamiltonian equation are $(Q_1(t), P_1(t))$ and $(Q_2(t), P_2(t))$, and the numerical solutions are, $(\tilde{Q}_1(t), \tilde{P}_1(t))$ and $(\tilde{Q}_2(t), \tilde{P}_2(t))$, with (5) satisfied.

In the case of asymmetric auxiliary distribution, the acceptance/rejection step is not in the simple format discussed in the HMC literature. In fact, to ensure the convergence to the right invariant measure, in this step, we will examine the following quantity,

$$\frac{\exp[-U(q_L)]}{\exp[-U(q_0)]} \times \frac{P(q_L, q_0)}{P(q_0, q_L)},$$

for a Markov chain step from state q_0 to state q_L , where $P(q_0, q_L)$ ($P(q_L, q_0)$) represents the transition probability to state q_L (q_0) from state q_0 (q_L). From the definition of our Markov chain, we have $P(q_0, q_L) = \exp(-V(p_0))$. This corresponds to the event that the auxiliary distribution takes the value of q_0 , and the Hamiltonian motion (or its numerical approximation) will map (q_0, p_0) to (q_L, p_L) . Meanwhile, $P(q_L, q_0)$ represents the event that the auxiliary distribution will take the value of certain $-p_L^*$, which is in general not equal to $-p_L$, as in the symmetric case. The proposed move will be accepted when,

$$\xi \leq \min \left\{ \frac{\exp[-U(q_L) - V(-p_L^*)]}{\exp[-U(q_0) - V(p_0)]}, 1 \right\}.$$

with ξ being an independent uniform $[0, 1]$ random variable. Furthermore, denote $-p_L^{**}$ as the momentum such that $(q_0, -p_L^{**})$ is the end of the Hamiltonian motion started from $(q_L, -p_L^*)$. Hence,

$$H(q_L, -p_L^*) = H(q_0, -p_L^{**}). \quad (9)$$

For any pair (q_1, q_2) , let,

$$\begin{aligned} \xi_1 &:= \frac{\exp[-U(\tilde{Q}_1) - V(-\tilde{P}_1^*)]}{\exp[-U(q_1) - V(p)]}, \\ \xi_2 &:= \frac{\exp[-U(\tilde{Q}_2) - V(-\tilde{P}_2^*)]}{\exp[-U(q_2) - V(p)]}. \end{aligned}$$

For any pair of initial states (q_1, q_2) , drawing the same auxiliary sample p , we have the following different cases for the acceptance/rejection scenarios,

- $\xi > \xi_1$ and $\xi > \xi_2$. In this case, both moves are rejected, the Wasserstein distance (conditioned on this event) will remain to be $\mathfrak{d}(q_1, q_2)$.
- $\xi \leq \xi_1$ and $\xi \leq \xi_2$. This comes back to the exact case with a small perturbation, (5) will guarantees that it will not affect the main result;
- $\xi \leq \xi_1$ and $\xi > \xi_2$. $\xi \leq \xi_1$ and $\xi > \xi_2$. The probability of this happening is equal to $\xi_1 - \xi_2$, From (9), we see that,

$$\xi_1 - \xi_2 = \exp[V(p)] \left\{ \exp[-V(-\tilde{P}_1^{**})] - \exp[-V(-\tilde{P}_2^{**})] \right\}.$$

By the same techniques, bounding the quantities through the integral, used in proving Lemma 2, we can write,

$$\left| \exp[-V(-P_1^{**})] - \exp[-V(-P_2^{**})] \right| = \int_0^1 -\exp[-V]V'(P^{**}(s)) \left| \frac{\partial p^{**}}{\partial q}(s) \right| \mathfrak{d}(q_1, q_2) ds.$$

From the definition of the momentum p^{**} , we know that the quantity $\frac{\partial p^{**}}{\partial q}(s)$ will be the product of $\frac{\partial Q}{\partial q}$ and $\frac{\partial P}{\partial q}$, where the first derivative represent the dependence of q_L on q_0 , and the second one represents the dependence of p^{**} on q_L . By the solution provided in Proposition 1, $\frac{\partial Q}{\partial q}$ is a bounded quantity (≤ 1) and $\frac{\partial P}{\partial q}$ can be bounded by a linear function of t , since the function sinc is bounded when the variable is small. Therefore, a carefully chosen T will guarantee

$$\exp[V(p)] \{ \exp[-V(-P_1^{**})] - \exp[-V(-P_2^{**})] \} < \frac{\beta}{2q_e} \mathfrak{d}(q_1, q_2),$$

for some $\beta < 1$, q_e is the average displacement of the Markov chain. The quality of approximation (5), thus guarantees that,

$$\exp[V(p)] \left\{ \exp[-V(-\tilde{P}_1^{**})] - \exp[-V(-\tilde{P}_2^{**})] \right\} < \frac{\beta'}{2q_e} \mathfrak{d}(q_1, q_2),$$

for some $\beta' < 1$. Combined, this will lead to that, on this scenario, $W_1(\mu(q_1), \mu(q_2)) \leq \beta' \mathfrak{d}(q_1, q_2)$.

- $\xi > \xi_1$ and $\xi \leq \xi_2$. The treatment is the same as the previous case.

In summary, if the acceptance/rejection decisions are the same for the exact and numerical solution, the closeness of the numerical integrator (5) ensures that the drift condition will be satisfied; meanwhile, (5) can also help to bound that the probability of the scenario that the acceptance/rejection decisions are different such that the drift condition can also be satisfied, as demonstrated in the last two cases above. Hence, there is a proper $\beta' < 1$ such that, $W_1(\mu(q_1), \mu(q_2)) \leq \beta' \mathfrak{d}(q_1, q_2)$, which implies the desired geometric convergence in Wasserstein distance. \square

B Numerical Experiments

Section B.1 describes additional experiments conducted with the simulation target distribution in \mathbb{R}^3 used in Section 5 of the paper. The same section also describes the ‘**adapt-single**’ and ‘**adapt-many**’ procedures to construct auxiliary distributions, where the first always constructs a Gaussian auxiliary and the second may construct an asymmetric auxiliary as mixtures of Gaussians. The target used there is constructed as a mixture of multiple Gaussians placed along three linearly independent directions (the final section provides details). The advantages of the ‘**adapt-many**’ procedure are sustained by these experiments, see **Fig. 3**.

In Section B.2, we provide experimental results from a different \mathbb{R}^3 simulation target. In this case, masses are placed along a helical curve. The ‘**adapt-many**’ procedure clearly displays its advantages over the existing methods, see **Fig. 5**.

In Section B.3, the final set of experiments were conducted in \mathbb{R}^3 using the same helical target. The results show the importance of using the AD-HMC method with asymmetric auxiliary distribution to ensure better performance, see **Figs. 6** and **7**.

In Section B.4, we provide detailed specifications of the Bayesian Logistic Regression model studied in Section 5, the results of which were presented in **Fig. 2**, specifications of each of the target distributions used in the simulation experiments in \mathbb{R}^3 , and a description of the leapfrog numerical procedure.

B.1 Varying Leapfrog Step size ϵ

A representation of the target distribution is displayed in **Fig. 4** (left). Recall that the experiments in **Fig. 1** were conducted with a stepsize of $\epsilon = 0.025$ for the Leapfrog numerical integrator. **Fig. 3** provides corresponding results when the stepsize in each iteration is increased to $\epsilon = 0.05$ while holding the number of steps $L = 100$ constant. The ordering behaviour of the HMC methods with symmetric auxiliaries is remarkably affected. While

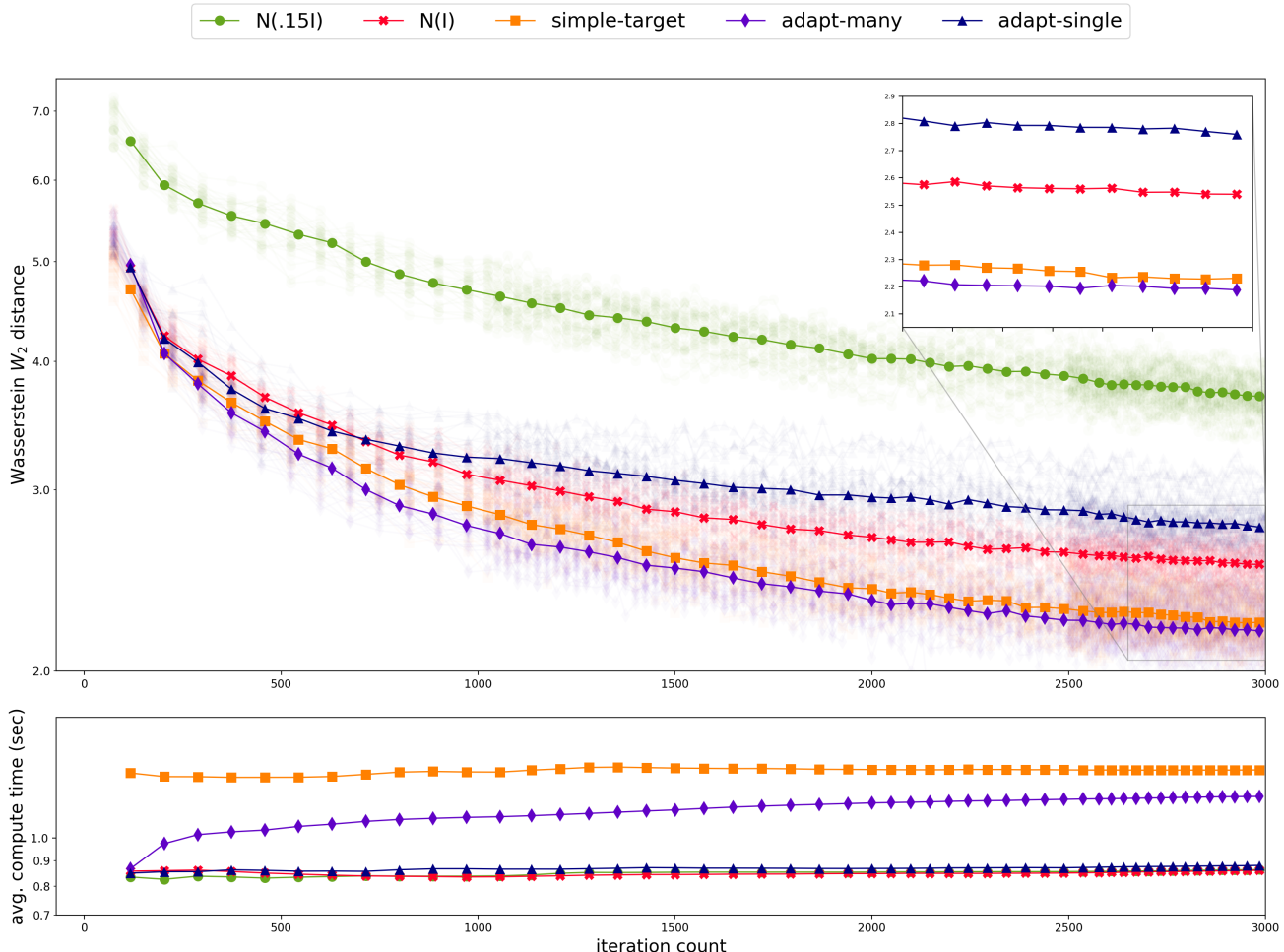


Figure 3: Performance of the three HMC ($N(I)$, $N(.15I)$ and adapt-single) and two AD-HMC (adapt-many and simple-target) settings of the W_2 distance between the iterate and the target distribution over (top) iteration counts and (bottom) average CPU wallclock times in seconds. Each method uses the Leapfrog integrator to implement Hamiltonian motion with $\epsilon = 0.05$, $L = 100$.

the $N(I)$ case continues to provide good performance, the auxiliaries $N(.15I)$ and adapt-single that skew their covariance matrices to match the steepness of the curvature of the potential energy (arising from the target) do not perform well. This is a well observed shortcoming of such auxiliaries with numerical integrators like the Leapfrog method. In practice, greater attention is paid to the degradation in performance as a factor of ϵ , and the parameter requires fine tuning to determine an appropriate value for each study. On the other hand, notice that the two AD-HMC methods perform just as well with this larger step-size as in with the adapt-many method significantly outperforming the other two practical methods ($N(I)$ and adapt-single). This regularization of performance is likely due to the inclusion of multiple Gaussians in their mixtures with a marked three-dimensional orientation of their means and a diverse set of covariance matrices. Note again that like the **Fig.** the adapt-many procedure picks up additional Gaussians as the iterations progresses, increasing its per-iteration cost.

B.2 Performance over second \mathbb{R}^3 target

We include a set of experiments now with a different target distribution, as displayed in **Fig.** 4 (right). This target places seven uncorrelated Gaussians with distinct variances along an expanding helical curve. **Fig.** 5 provides the performance of the three practical (no prior knowledge) methods, the $N(I)$ and adapt-single HMC methods and the adapt-many AD-HMC method. The orientation of the smaller number of Gaussians in the mixture that

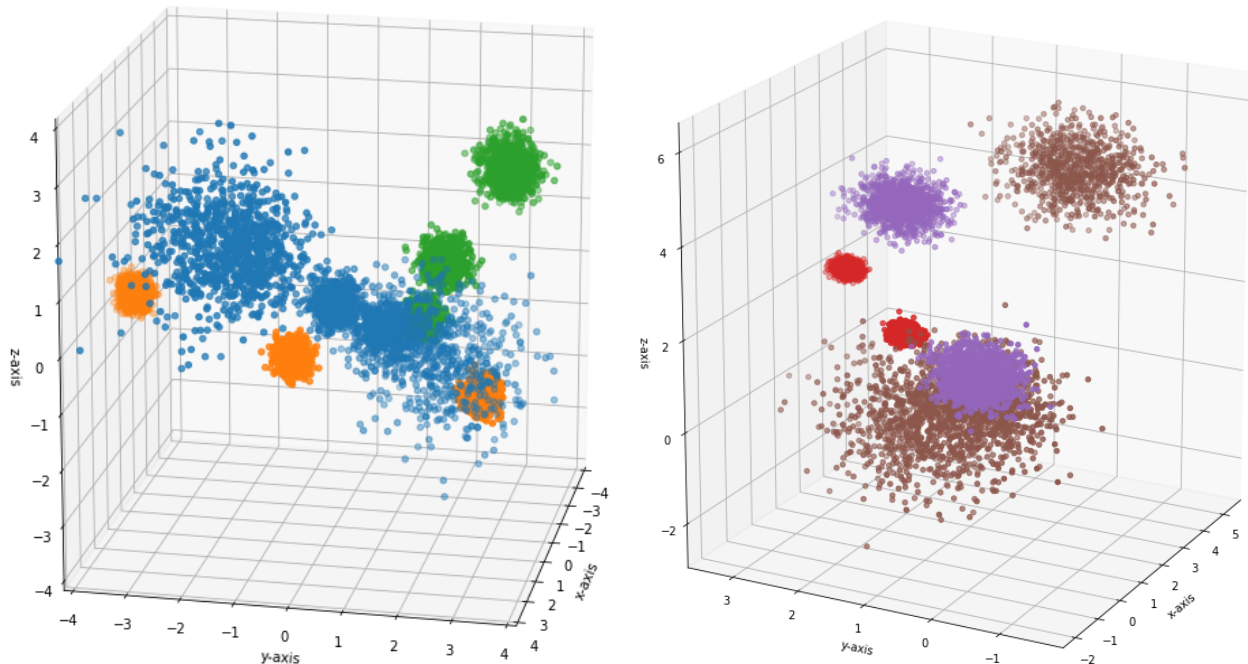


Figure 4: The two \mathbb{R}^3 target distributions are displayed using samples. *Left*: The target distribution used in **Figs. 1, 3 and, 6** centers twelve Gaussians on three linearly independent directions, as indicated by the masses with the three colors. In addition, the (uncorrelated) Gaussians have a range of variances from $[0.15, 1.0]$. *Right*: The target distribution used in **Figs. 5 and 7** centers seven (uncorrelated) Gaussians along an expanding helical curve. The varying standard deviations are indicated with the three colors.

constitutes the target has led to a dramatic difference in performance of the two adaptive schemes, which is seen to have been achieved by the AD-HMC scheme with only a modest increase in computational effort; indeed, on average the number of clusters in the mixture is an even split between two and three over the 30 replications.

B.3 AD-HMC vs HMC for Asymmetric $g(p)$

Finally, we address the question of whether the direction reversal in AD-HMC matters in practice by comparing Algorithm 2 with the forward-motion-only standard HMC in Algorithm 1 when using different momentum distributions.

Recall from the discussion preceding Theorem 1 that when the auxiliary $g(p)$ is symmetric, the corresponding Hamiltonian operator is self-adjoint; in other words, forward and backward motions produce distributionally identical outcomes. On the other hand, it is unclear whether the iterations make any progress when the auxiliary $g(p)$ is asymmetric and only the forward motion HMC is implemented. **Figs. 6 and 7** illustrate this vividly for the case of the first simulation targets in \mathbb{R}^3 . In each experiment, the ‘*adapt-many*’ heuristic is implemented both with the forward-motion-only HMC and the alternating direction (AD-)HMC algorithms. Notice that in each case, the performance is remarkably poorer when only using forward-moving HMC as against the AD-HMC, with the second target’s HMC iterations making no progress at all. The results demonstrate vividly the necessity of the AD-HMC over HMC for asymmetric momentum distributions. Table 1 shows that this impact is due to an order of magnitude more moves being rejected under the HMC than under AD-HMC.

B.4 Experiment details

Bayesian Logistic Regression.

The logistic regression model seeks to explain the outcomes of binary-valued random variable $Y \in \{0, 1\}$ using features $X = (x_1, x_2, \dots, x_d)$. In particular, if $p = P(Y = 1)$, then the model chooses the best q for this relation

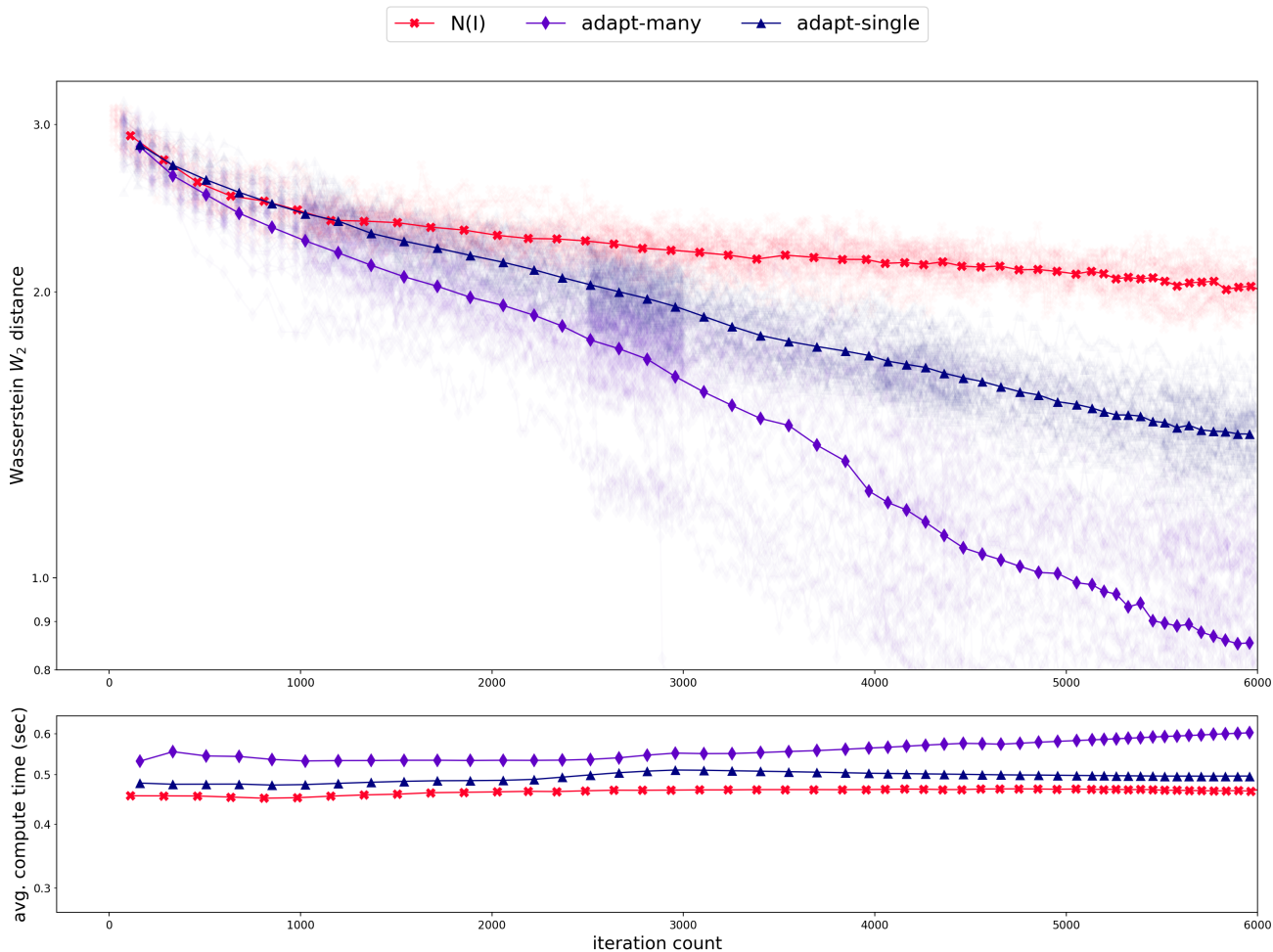


Figure 5: Performance of the three HMC (‘ $N(I)$ ’, ‘ $N(.15I)$ ’ and ‘**adapt-single**’) and two AD-HMC (‘**adapt-many**’ and ‘**simple-target**’) settings of the W_2 distance between the iterate and the target distribution over (top) iteration counts and (bottom) average CPU wallclock times in seconds. Each method uses the Leapfrog integrator to implement Hamiltonian motion with $\epsilon = 0.05$, $L = 100$.

	Fig. 6	Fig. 7
HMC	0.13 ± 0.02	0.02 ± 0.00
AD-HMC	0.92 ± 0.01	0.74 ± 0.02

Table 1: Comparison of the average fraction of rejected samples from the HMC and AD-HMC methods implementing the ‘**adapt-many**’ heuristic. The first two columns present confidence intervals (CI) for **Fig. 6** and the last two columns present CIs for **Fig. 7**.

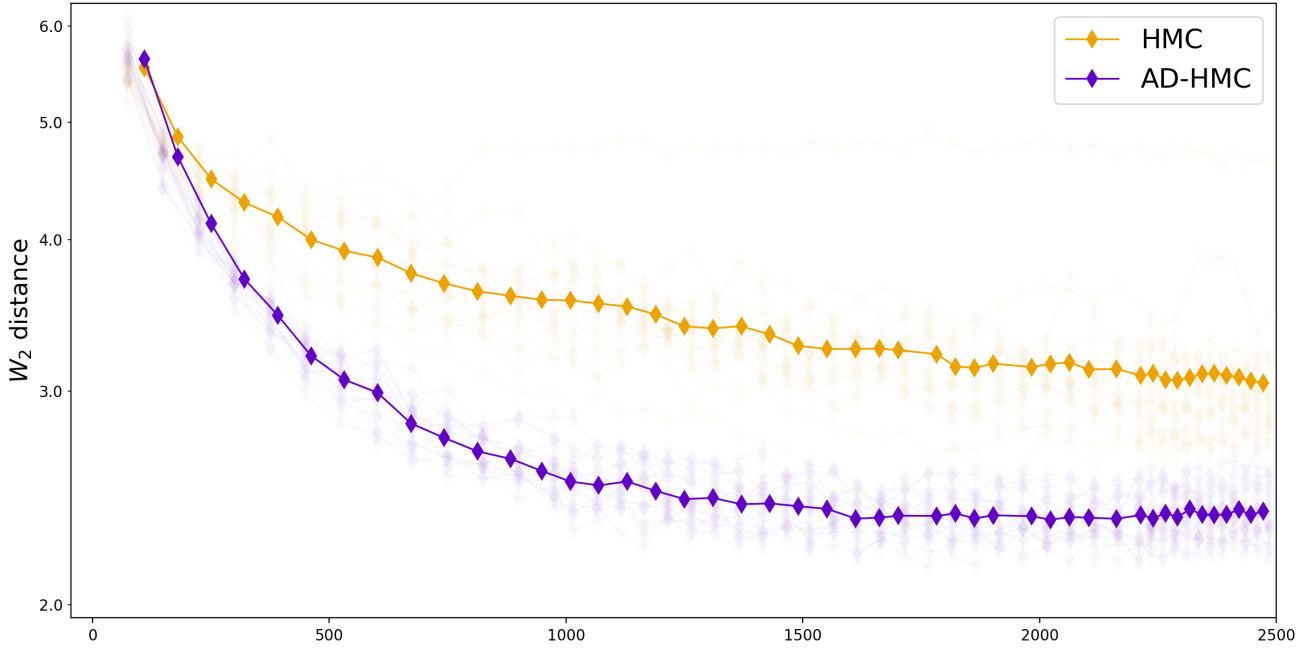


Figure 6: Performance of the (‘`adapt-many`’) heuristic using forward-motion-only HMC and AD-HMC for the target in f as **Figs. 1** and **3**: W_2 distance between the iterate and the target distribution over (top) iteration counts and (bottom) average CPU wallclock times in seconds. Each method uses Leapfrog integrator to implement Hamiltonian motion with $(\epsilon, L) = (0.025, 100)$.

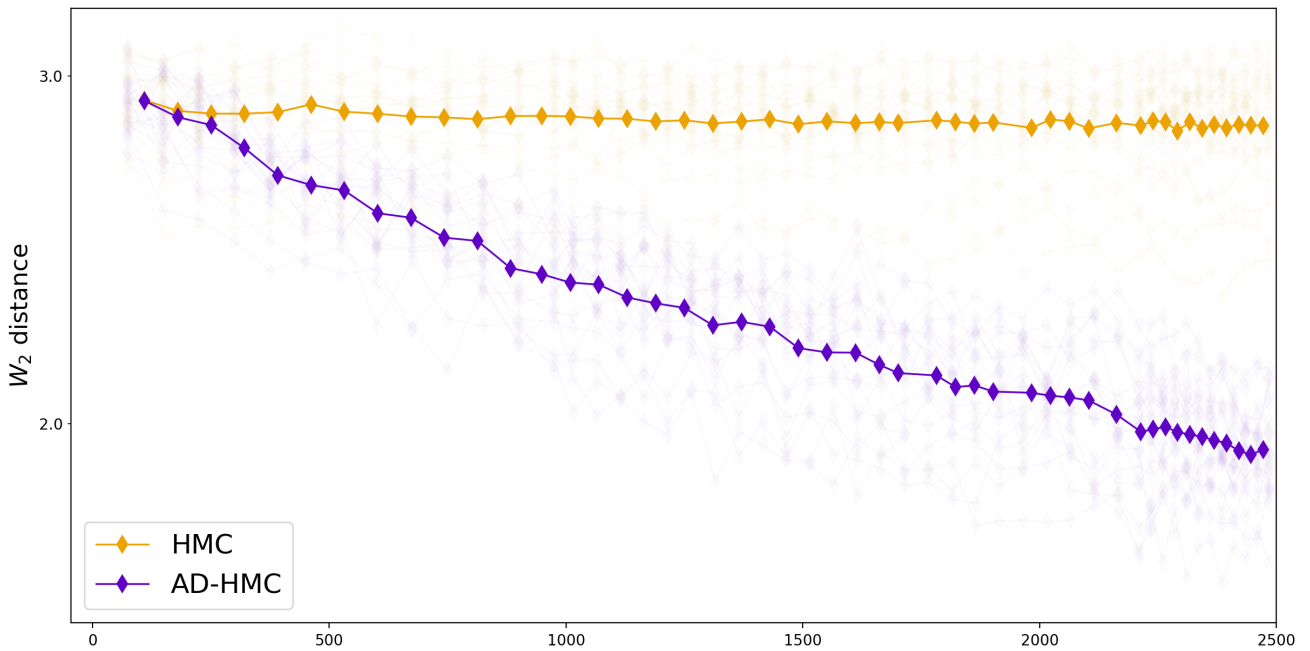


Figure 7: Performance of the (‘`adapt-many`’) heuristic using forward-motion-only HMC and AD-HMC for the same target as **Fig. 5**: W_2 distance between the iterate and the target distribution over (top) iteration counts and (bottom) average CPU wallclock times in seconds. Each method uses the Leapfrog integrator to implement Hamiltonian motion with $\epsilon = 0.05, L = 100$.

to hold:

$$\log \frac{p}{1-p} = q^t X,$$

where q is called the regression parameter. (For completeness, assume that the first component of X is always 1 in order to capture the intercept of this linear regression.) Correspondingly, the probability p is given by the *logistic* or *sigmoid* function

$$p = p(q^t X) := \frac{1}{1 + e^{-q^t X}}. \tag{10}$$

Let $\mathbf{T} := \{(X_n, Y_n), n = 1, \dots, N\}$ be a collection of features and observed outcomes over which the best q is to be trained. Bayesian analysis of this model starts with a prior distribution $\pi(q)$ on q , and searches for the the posterior $\mathbb{P}(q|\mathbf{T})$ given the training set \mathbf{T} . This is defined up to the normalizing constant via the Bayes relation

$$\mathfrak{f}(q) := \mathbb{P}(q|\mathbf{T}) \propto \pi(q)\mathbb{P}(\mathbf{T}|q),$$

where $\mathbb{P}(\mathbf{T}|q)$ is the *likelihood* of \mathbf{T} for a given regression parameter q :

$$\mathbb{P}(\mathbf{T}|q) = \prod_{n=1}^N p(q^t X_n)^{Y_n} (1 - p(q^t X_n))^{(1-Y_n)} = \prod_{n=1}^N \frac{e^{(q^t X_n) Y_n}}{1 + e^{q^t X_n}}.$$

In particular, the gradient of potential $U(q)$ of $\mathfrak{f}(q)$ is

$$\nabla_q U(q) = -\frac{1}{\pi(q)} \nabla_q \pi(q) + \sum_{n=1}^N (p(q^t X_n) - Y_n) X_n, \tag{11}$$

where $p(\cdot)$ is the sigmoid function defined in (10).

Fig. 2 applies HMC using the gradient (11) to the dataset obtained from Huq and Cleland (1990), where the authors present responses to a questionnaire from 1934 female respondents. The following variables are presented for each respondent:

- **livch**: Number of living children at time of survey. Levels are 0, 1, 2, 3+
- **age**: Age of woman at time of survey (in years), centred around mean.
- **urban**: Type of region of residence. Levels are urban and rural
- **use**: Contraceptive use at time of survey.

We seek to train the probability of contraceptive **use** over the three factors **livch**, **age** and **urban**. Along with the intercept term, this yields a Bayesian inference problem for the posterior $\mathbb{P}(q|\mathbf{T})$ for $q \in \mathbb{R}^4$. The prior distribution is set to be $\pi(q) \sim N(\mathbf{0}, 10.0^2 I)$ in our experiments. Finally, we measure the progress in the iterations using the Kuhlback-Leibler distance between iterate h_n and the posterior \mathfrak{f} :

$$d_{KL}(h_n, \mathfrak{f}) = \int h_n(q) \log \frac{h_n(q)C}{\pi(q)\mathbb{P}(\mathbf{T}|q)} dq = d_{KL}(h_n, \pi) - \mathbb{E}_{h_n}[\log \mathbb{P}(\mathbf{T}|q)] + \log C,$$

where the last term containing the (unknown) normalizing constant C is ignored in our calculations.

Simulation Target Distributions.

The target distribution used in the **Figs. 1, 3** and **6**, displayed in **Fig. 4** on the left, is selected as the mixture:

$$f(q) = \begin{cases} N([2.48, 1.75, 1.75], 0.75^2 I) & 0.058 \\ N([1.77, -1.25, 1.25], 0.50^2 I) & 0.058 \\ N([0.00, 0.00, 0.00], 0.25^2 I) & 0.058 \\ N([-1.06, 0.75, -0.75], 0.25^2 I) & 0.058 \\ N([-1.41, 1.00, -1.00], 0.50^2 I) & 0.033 \\ N([-2.47, 1.75, -1.75], 0.75^2 I) & 0.067 \\ N([3.75, 0.00, 0.15], 0.15^2 I) & 0.11 \\ N([4.00, 3.46, -0.20], 0.15^2 I) & 0.11 \\ N([0.63, -3.68, 0.10], 0.15^2 I) & 0.11 \\ N([2.04, 2.07, 0.47], 0.15^2 I) & 0.11 \\ N([1.64, 2.40, 1.35], 0.20^2 I) & 0.11 \\ N([0.59, 3.35, 2.77], 0.25^2 I) & 0.11 \end{cases}$$

Note that all the correlation matrices are held to be the identity matrix I (that is, the components are uncorrelated) and variances in all three dimensions are scaled equally. The asymmetric auxiliary ‘simple-target’ used in **Fig. 1** is the mixture:

$$g(p) = \begin{cases} N([-0.68, 1.33, -1.33], 0.75^2 I) & 0.17 \\ N([0.68, -1.33, 1.33], 0.25^2 I) & 0.17 \\ N([-0.00, -2.00, -0.00], 0.15^2 I) & 0.17 \\ N([0.00, 2.00, 0.00], 0.15^2 I) & 0.17 \\ N([0.87, -1.00, -1.50], 0.25^2 I) & 0.17 \\ N([-0.87, 1.00, 1.50], 0.15^2 I) & 0.17 \end{cases}$$

The target distribution (displayed in **Fig. 4** (right)) utilized in **Figs. 5** and **7** is selected as the mixture:

$$f(q) = \begin{cases} N([0.00, 1.00, 0.00], 0.69^2 I) & 0.14 \\ N([0.15, 0.15, 0.79], 0.49^2 I) & 0.14 \\ N([-0.57, -0.00, 1.57], 0.29^2 I) & 0.14 \\ N([-0.96, 0.96, 2.36], 0.10^2 I) & 0.14 \\ N([-0.00, 2.14, 3.14], 0.10^2 I) & 0.14 \\ N([2.07, 2.07, 3.93], 0.29^2 I) & 0.14 \\ N([3.71, 0.00, 4.71], 0.49^2 I) & 0.14 \end{cases}$$

Numerical Approximation of AD-HMC

A closed-form expression for the Hamiltonian motion is not readily available for general target and (asymmetric) momentum distributions, and so we use the Leapfrog or Störmer–Verlet first-order numerical integration method Verlet (1967). The Leapfrog method interleaves discrete momentum (p) and position (q) variable updates in a sequence of steps where only one variable changes at a time, and hence the Jacobian of the transformation ensures that volume is preserved in the (q, p) space. The method takes L steps each of size ϵ to move a path of length $T = L\epsilon$. Starting at a point $(Q(0), P(0)) = (q_0, p_0)$, the leapfrog procedure repeats the following for $l = 0, \dots, L - 1$:

$$\begin{aligned} P\left(l\epsilon + \frac{\epsilon}{2}\right) &= P(l\epsilon) - \frac{\epsilon}{2} \frac{\partial H}{\partial q}(Q(l\epsilon), P(l\epsilon)), \\ Q(l\epsilon + \epsilon) &= Q(l\epsilon) + \epsilon \frac{\partial H}{\partial p}\left(Q(l\epsilon), P\left(l\epsilon + \frac{\epsilon}{2}\right)\right), \\ P(l\epsilon + \epsilon) &= P\left(l\epsilon + \frac{\epsilon}{2}\right) - \frac{\epsilon}{2} \frac{\partial H}{\partial q}(Q(l\epsilon + \epsilon), P(l\epsilon + \frac{\epsilon}{2})). \end{aligned}$$

This integrator ensures that the difference $|H(Q(T), P(T)) - H(q_0, p_0)|$ grows slowly with ϵ and L . A replacement of the exact Hamiltonian motion steps in Algorithms 1 and 2 however is still an approximation HMC procedure

that converges (fast in many cases, as per Theorem 4) to a distribution close to $f(q)$. To recover an MCMC procedure that ensures convergence to the desired limit $f(q)$ exactly, the standard practice is to embed this approximate HMC motion into a Metropolis-Hastings scheme as a candidate proposal mechanism. So, an additional step is carried out where the candidate new iterate $(Q(T), P(T))$ is accepted with probability

$$\min \left\{ 1, \frac{f(Q(T))g(P(T))}{f(q_0)g(p_0)} \right\} = \min \{ 1, \exp (-U(Q(T)) - V(P(T)) + U(q_0) + V(p_0)) \}.$$

The stepsize ϵ is chosen carefully, and in practice varied with the current iterate as the local curvature of the Hamiltonian H dictates, so that the proportion of samples rejected by this step is minimal.